Assessment of the Potential Anti-Proliferative Effects of Margaritaria Discoidea Extract on a Rat Model of Benign Prostate Hyperplasia

Bernard Opeyemi Adedeji
Department of Physiology, Federal University of Health Sciences
David Tolulope Oluwole
Department of Physiology, Crescent University
Moses Agbomhere Hamed
The Brainwill Laboratory
Oyedayo Phillips Akano
Department of Physiology, Olabisi Onabanjo University
Ayodeji Folorunsho Ajayi
aajayi22@lautech.edu.ng

Department of Physiology, Ladoke Akintola University of Technology

Research Article

Keywords: Anti-proliferative, Benign Prostatic Hyperplasia, Inflammation, Oxidative stress, Phyto-therapy

Posted Date: April 14th, 2026

DOI: https://doi.org/10.21203/rs.3.rs-9258984/v1

Additional Declarations: No competing interests reported.

ASSESSMENT OF THE POTENTIAL ANTI-PROLIFERATIVE EFFECTS OF *Margaritaria discoidea* EXTRACT ON A RAT MODEL OF BENIGN PROSTATE HYPERPLASIA

Bernard Opeyemi Adedeji[1,5], Oluwole David Tolulope[2], Moses Agbomhere Hamed[3,7], Oyedayo Phillips Akano[4], Ayodeji Folorunsho Ajayi[5,6*],

[1]Department of Physiology, Federal University of Health Sciences, Ila-Orangun, Osun-State, Nigeria.

[2]Department of Physiology, Crescent University, Abeokuta, Ogun State, Nigeria.

[3] The Brainwill Laboratory, Osogbo, Osun State, Nigeria.

[4]Department of Physiology, Olabisi Onabanjo University, Ago Iwoye, Ogun State, Nigeria;

[5]Department of Physiology, Ladoke Akintola University of Technology, Ogbomoso, Oyo State, Nigeria;

[6]Anchor Biomed Research Institute, Ogbomoso, Oyo State, Nigeria;

[7]Department of Medical Laboratory Science, Afe Babalola University, Ado-Ekiti, Ekiti State. Nigeria.

[*]**Corresponding author:**
Professor Ajayi Ayodeji Folorunsho,
Department of Physiology,
Ladoke Akintola University of Technology, PMB 4000, Ogbomoso, Nigeria.
+2348033834495 Email: aajayi22@lautech.edu.ng

ABSTRACT

Benign prostatic hyperplasia (BPH) is a prevalent condition in men over 50, often developing into malignant tumors. Current treatments, including surgery and pharmacological interventions, have side effects like erectile dysfunction and depression. This study explored the anti-proliferative effect of aqueous extract of M. discoidea stem bark (AESBM) in a rat model of BPH. Twenty male rats were randomized into four groups (n=5): control, untreated BPH, finasteride-treated, and AESBM-treated. GC-MS analysis of AESBM revealed methyl benzoate, methyl palmitate, and methyl stearate as abundant constituents, with molecular docking studies showing strong 5AR2 inhibition. BPH was induced by testosterone propionate injection for 28 days, and AESBM was administered orally for 28 days. BPH induction increased prostate weight, PSA, and testosterone levels, accompanied by increased IL-6, TNF-α, IL-1β, NO, and caspase 3, and decreased antioxidant activities. These events were associated with glandular and stromal hyperplasia. Treatment with AESBM abrogated these oxido-inflammatory-mediated apoptotic responses, with effects comparable to finasteride. Findings from this study established the efficacy of AESBM as a potential phytotherapeutic agent for BPH management. AESBM's ameliorative effects suggest its potential as a natural therapeutic option for BPH, warranting further investigation. The study's results highlight the importance of exploring natural products for BPH treatment.

Keywords: Anti-proliferative, Benign Prostatic Hyperplasia, Inflammation, Oxidative stress, Phyto-therapy

1. INTRODUCTION

Benign prostatic hyperplasia (BPH) is one of the most prevalent urological disorders in aging men, with its incidence progressively rising with advancing age and manifesting as lower urinary tract symptoms (LUTS) that significantly impair patients' quality of life (Gravas et al., 2023; Wang et al., 2024). This condition is defined by a non-neoplastic enlargement of the prostate gland resulting from hyperproliferation of epithelial and stromal components, potentially attributed to vascular senescence, persistent inflammatory processes, and age-related androgen decline (Phua, 2021). The pathogenesis of BPH is multifactorial, with key contributing factors including hormonal imbalances—particularly the accumulation of dihydrotestosterone (DHT)—oxidative stress, chronic inflammation, and metabolic disorders such as obesity and insulin resistance Benign prostatic hyperplasia (BPH) commonly causes gradual narrowing of the urethral lumen, giving rise to lower urinary tract symptoms (LUTS)

including urgency, increased frequency, nocturia, and diminished urinary stream (Gravas et al., 2023). Its incidence rises with advancing age, occurring in approximately half of men in their fifties and reaching up to 90% in individuals over 80 years (Roehrborn et al., 2010; Phua, 2021).

Pharmacological interventions, including α-adrenergic receptor antagonists, 5-α reductase inhibitors (5ARIs), phosphodiesterase-5 inhibitors (PDE5Is), and their combined regimens (Fig. 1), provide effective symptomatic relief but are frequently linked with undesirable effects such as erectile dysfunction, dizziness, postural hypotension, and retrograde ejaculation Likewise, surgical and minimally invasive approaches, particularly transurethral resection of the prostate (TURP), are associated with potential complications including hemorrhage, infections, urinary incontinence, retrograde ejaculation, diminished libido, and infertility (Nickel et al., 2011; Corona et al., 2017; Young, 2021). Figure 1 present a graphical illustration of risk factors, diagnosis and management of BPH.

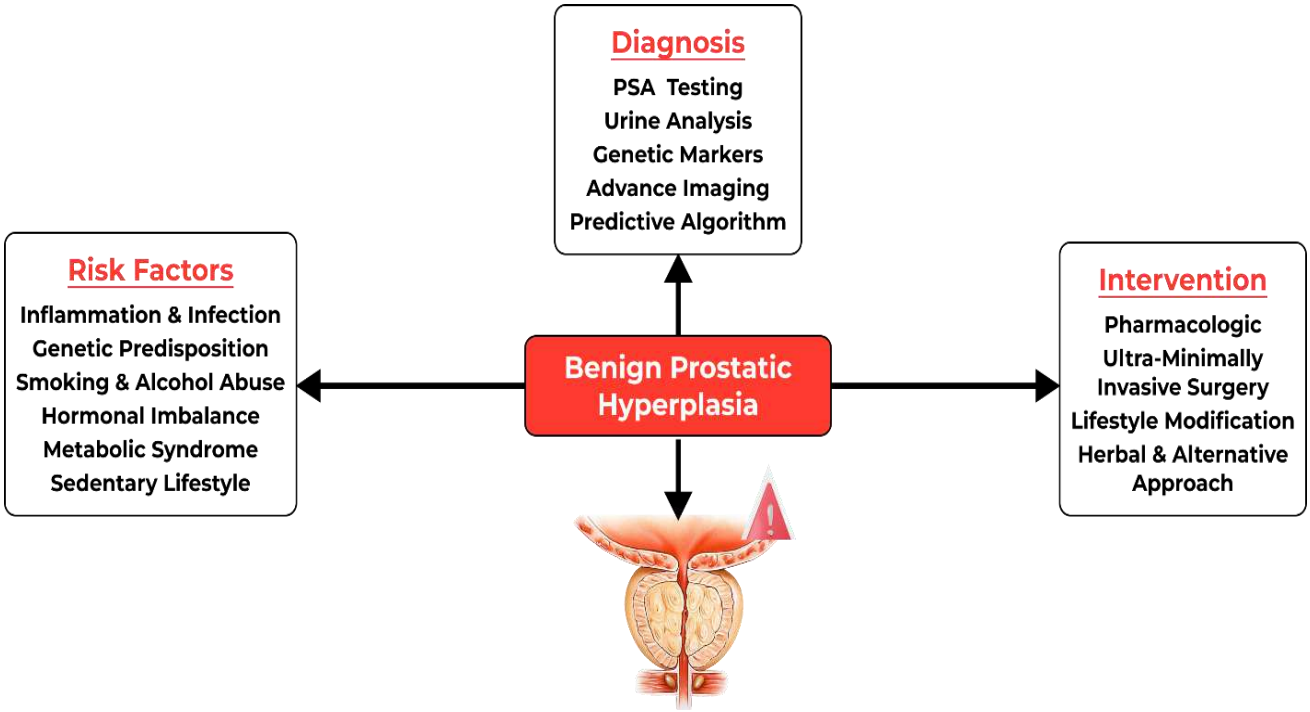

Figure 1: A graphical illustration of risk factors, diagnosis and management of BPH.

There is growing interest in the development of novel interventions to combat the proliferation of the prostate gland, and notably, phytotherapy offers a wealth of opportunities for drug discovery. The potential of phytotherapy is holistic, with possible anti-androgenic, anti-proliferative, anti-inflammatory, antioxidant, anti-apoptotic, and cytotoxic properties (Gwedela et al., 2022). Given the limitations of conventional therapies, there is increasing interest in exploring alternative treatments, particularly medicinal plants with potential therapeutic benefits. While phytotherapies like saw palmetto (*Serenoa repens*) (Agbabiaka et al., 2009) and *Pygeum africanum* (Wilt et al., 2002) are increasingly explored for BPH, their clinical adoption remains limited due to inconsistent efficacy in trials, non-standardized extracts, and poorly characterized mechanisms of action. This underscores the need to investigate alternative plants like *Margaritaria discoidea*, which offers a unique phytochemical profile with documented anti-inflammatory and antioxidant properties, yet remains understudied for prostate health.

Margaritaria discoidea commonly known as "*Igi Awewe" and "Igi Oko*" is a plant widely used in African herbal medicine that has demonstrated anti-inflammatory, antioxidant, and cytotoxic properties (Ekuadzi et al., 2018; Gwedela et al., 2022), making it a promising candidate for managing BPH. However, its specific effects on prostate health remain largely unexplored. This study seeks to assess the potential anti-proliferative effects of *Margaritaria discoidea* extract in a rat model of BPH, thereby contributing to the scientific understanding of its role in prostate health. Figure 1 is a graphical illustration of risk factors, diagnosis and management of BPH.

2.0 Materials and methods

Ethical Approval

Ethical approval for this research was obtained from the Research Ethics Review Committee, Faculty of Basic Medical Sciences, Ladoke Akintola University of Technology (LAUTECH), Oyo State (ERCFBMSLAUTECH:089/01/2025).

2.1 Chemicals and drug

Testosterone propionate (TP) used for the induction of BPH was obtained from Sigma-Aldrich Chemical Company, Germany, while Finasteride was sourced from Aurobindo Pharma - Milpharm Ltd., United Kingdom. All additional chemicals and reagents utilized in this investigation were of analytical grade.

2.2 Collection of Plant and Preparation of Plant Extract

The stem bark of *Magaritaria discoidea* was collected from the Osun State College of Education, Ila Orangun, Nigeria and the plant was authenticated at the Department of Biology, Ladoke Akintola University of Technology, Ogbomosho, Oyo state, Nigeria, with voucher number LAUH-2243 deposited in the university herbarium.

The freshly harvested bark was thoroughly cleaned by rinsing under running water to eliminate soil particles and debris after which it was air-dried at ambient temperature (22–25 °C) for about 14 days in a well-ventilated environment, shielded from direct sunlight to preserve thermo-labile constituents. The dried material was subsequently pulverized into a fine powder using a heavy-duty mechanical grinder, yielding a total of 30 kg of stem bark powder.

Plant extraction was done using the decoction method described by Kumar et al. (2010). The 30 kg of powdered plant material was soaked in distilled water (10 L per kg; total of 300 L) for 24 hours with intermittent stirring to facilitate the release of bioactive compounds. The mixture was then decanted and filtered using a clean, double-layered muslin cloth to separate the aqueous extract from plant residues. The filtrate was concentrated using a rotary evaporator (Büchi R-300) under reduced pressure at 45 °C to remove excess water, followed by final drying in a hot-air oven at the same temperature to obtain a semi-solid extract. The total yield was approximately 2 kg of dark brown extract, representing a 6.7% w/w yield from the initial powdered material.

2.3 Gas chromatography and Mass Spectrometry (GC-MS) of Plant Extract

The plant material was immersed in absolute ethanol within a plain tube and subjected to a 5-minute ultrasonic treatment in a water bath. The resulting supernatant was filtered through a 0.45 μm membrane, and a 100 μL aliquot of the filtrate was used for GC-MS analysis. The aqueous extract underwent GC-MS profiling using an Agilent 5977B GC/MSD system coupled with an Agilent 8860 autosampler (Dagar et al., 2024), The system featured a gas chromatograph linked to a mass spectrometer, equipped with an Elite-5MS fused silica capillary column (30 m × 0.25 mm ID × 0.25 μm film thickness), utilizing 5% diphenyl and 95% dimethyl polysiloxane as the stationary phase. Operating conditions included electron ionization (EI) at 70 eV, helium carrier gas (99.999% purity) at 1 mL/min, and 1 μL sample injection in split mode (10:1 ratio). Injector and ion source temperatures were set at 300 °C and 250 °C, respectively. The oven temperature was initially held at 100 °C for 0.5 minutes, ramped

at 20 °C/min to 280 °C, and held for 2.5 minutes. Mass spectra were acquired (45–450 Da, 0.5-second scan interval) with a 3-minute solvent delay (Agilent, 2019).

2.4 Insilico procedures

2.4.1 Target search and ligand preparation

In the initial part of the virtual screening protocol, Human steroid 5α-reductase 2 (SRD5A2), a transmembrane enzyme involved in steroid metabolism which is responsible for catalyzing the conversion of testosterone to dihydrotestosterone was retrieved (PDB: 7BW1) while the canonical SMILES of finasteride and the selected ligands were obtained from the Pubchem database, their 2D molecular structures generated using ChemDraw Ultra 8.0 (CambridgeSoft Corporation, USA, 2003), subsequently transformed into 3D conformations with Spartan software, followed by geometric optimization through the AM1 semi-empirical method with the optimized structures exported as pdb files, after which polar hydrogens were incorporated prior to Gasteiger charge assignment, partial atomic charges calculated via the Gasteiger-Marsili algorithm, nonpolar hydrogens merged, and rotatable bonds defined using AutoDock Tools (ADT) before saving the final structures in pdbqt format.

2.4.2 Protein preparation

The X-ray crystallographic structure (PDB ID: 7BW1, resolution 2.8 Å, R-free value 0.265) illustrated in Figure 2 was obtained from the Protein Data Bank (PDB). Molecular docking preparation was carried out using UCSF Chimera (Couch et al., 2006). . Prior to docking, amino acid residues within a distance of <5.0 Å from the bound ligand were identified, and the protein–ligand complex retrieved from PDB was refined by removing non-standard residues along with the co-crystallized dihydrofinasteride (DHF) from the three-dimensional structure. The separated DHF was prepared in Chimera and stored as Lig.mol2, while the corresponding receptor structure was processed and saved as rec.pdb.

The putative binding site was restricted to the catalytic domain of SRD5A2 and defined using AutoGrid (Morris et al., 2009). The structural outputs generated from Chimera were imported into AutoDock Tools (ADT) (Morris et al., 2009), , where a grid spacing of 0.375 Å was established and centered on the catalytic domain residues interacting with dihydrofinasteride. The grid box encompassed the entire DHF-binding region of SRD5A2, ensuring adequate conformational freedom for the ligands to adopt optimal binding orientations. Subsequently, the receptor (rec.pdb) and ligand (Lig.mol2) files were converted into the “pdbqt” format, which incorporates pdb coordinates with additional charge (“q”) and AutoDock type (“t”) information. For the macromolecule, polar hydrogen atoms were added, and Kollman United Atom charges together with solvation parameters were assigned. For the ligand, polar

hydrogens were introduced prior to calculating Gasteiger charges required for electrostatic interactions, after which nonpolar hydrogens were merged. Partial atomic charges were computed using the Gasteiger–Marsili algorithm (Gasteiger & Marsili, 1980), and the processed files were saved in pdbqt format. Figure 2 is a3D image of Human steroid 5α-reductase 2 (SRD5A2) (PDB: 7BW1).

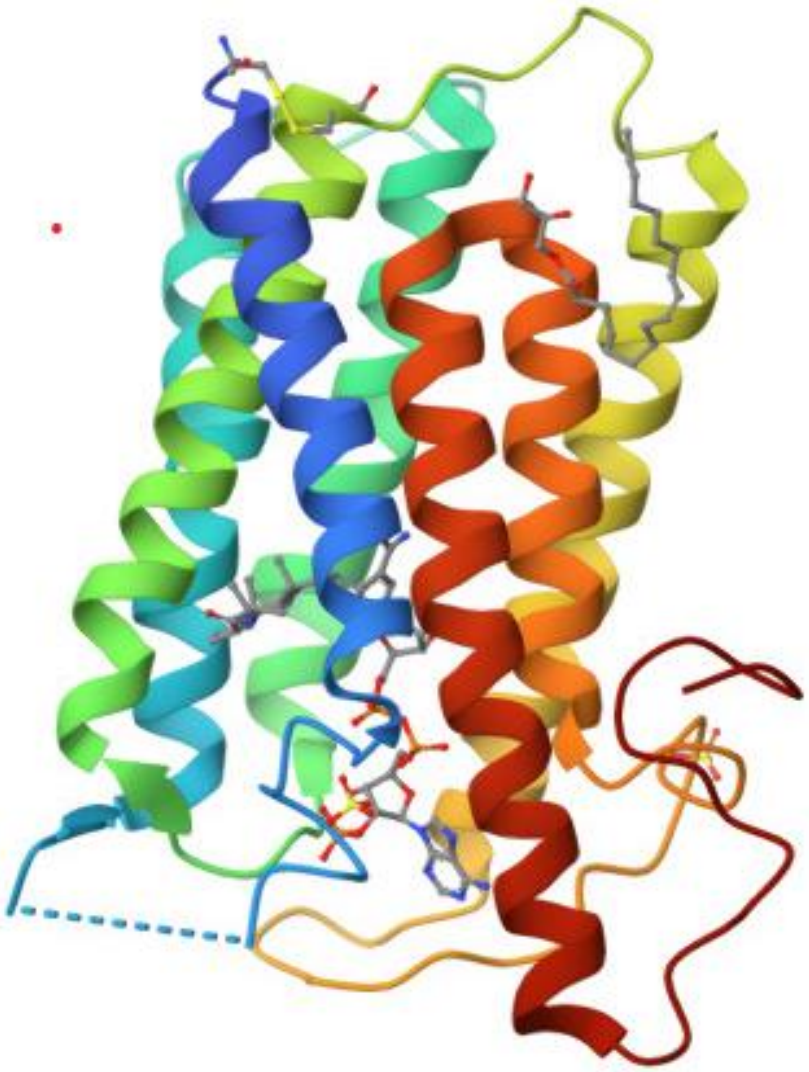

Figure 2: 3D image **of** Human steroid 5α-reductase 2 (SRD5A2) (PDB: 7BW1).

2.4.3 Docking Protocol

Dihydrofinasteride and the generated ligands candidate were submitted for Molecular docking against the SRD5A2 target (PDB ID: 7BW1). Molecular docking was performed considering a flexible ligand and rigid receptor as described by (Meng et al., 2011), using virtual screening software Auto Dock Vina (Trott & Olson, 2010).

The libraries of ligands were docked on the active site of the protein. The grid box parameter (-29.743, 15.318, 37.151) for (x, y, z) coordinates, respectively, with size (60, 40, 48) for (x, y, z) which covered the entire binding site of the protein is as shown on Table 1 and it is assumed to provide enough space for the ligands rotational and translational walk. The grid box parameter was used to write configuration file (config.txt). Auto Dock Vina generated results in the pdbqt.pdbqt format.

Compounds exhibiting favorable binding energy, optimal geometric conformation, and broad inhibition across the studied proteins were selected from Chimera's View Dock feature and saved in complex with the reference protein. To validate the docking protocol, the co-crystallized ligand was separated from each protein crystal structure and re-docked using the established parameters. The procedure yielding a conformation that closely matched the co-crystallized ligand's geometric conformation in the active site was selected. A 3D representation of Human steroid 5α-reductase 2 (SRD5A2) (PDB: 7BW1) is shown in Figure 2.

2.4.5 Drug-likeness and ADMET predictions

Using the pkCSM Web server (http://biosig.unimelb.edu.au/ pkcsm/prediction), multiple molecular descriptors were calculated to evaluate the absorption, distribution, metabolism, excretion, and toxicity (ADMET) characteristics of the proposed SRD5A2 inhibitors, while Lipinski’s rule of five was applied to determine their drug-likeness based on critical physicochemical parameters, including molecular weight, hydrogen bond acceptor count, hydrogen bond donor count, and the octanol–water partition coefficient (Pires et al., 2015; Yang et al., 2019).

Table 1: Basic information on finasteride and the generated ligand

S/N	Compound Name	PubChem ID	Molecular Formula	Canonical Smiles	Structure
0	Finasteride	57363	$C_{23}H_{36}N_2O_2$	C[C@]12CC[C@H]3[C@H]([C@@H]1CC[C@@H]2C(=O)NC(C)(C)C)CC[C@@H]4[C@@]3(C=CC(=O)N4)C	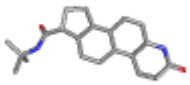
1	Undecane	14257	$C_{11}H_{24}$	CCCCCCCCCCC	
2	Benzoic acid, methyl ester	7150	$C_8H_8O_2$	COC(=O)C1=CC=CC=C1	
3	Benzoyl isothiocyanate	68284	C_8H_5NOS	C1=CC=C(C=C1)C(=O)N=C=S	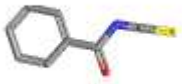
4	Hexadecanoic acid, methyl ester	8181	$C_{17}H_{34}O_2$	CCCCCCCCCCCCCCCC(=O)OC	
5	Dodecanoic acid, 10-methyl-, methyl ester	3014565	$C_{13}H_{26}O_2$	CCC(C)CCCCCCCCC(=O)O	
6	Methyl stearate	8201	$C_{19}H_{38}O_2$	CCCCCCCCCCCCCCCCCC(=O)OC	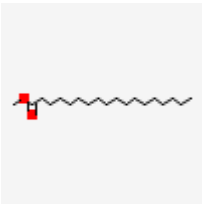

7	Oxirane, 2,2-dimethyl-3-(3,7,12,16,20-pentamethyl-3,7,11,15,19-heneicosapentaenyl)	5366020	$C_{30}H_{50}O$	CC(=CCC/C(=C/CC/C(=C/CC/C=C(\C)/CC/C=C(\C)/CCC1C(O1)(C)C)/C)/C)C	
8	2R-Acetoxymethyl-1,3,5-trimethyl-4c-(3-methyl-2-buten-1-yl)-1c-cyclo hexanol	550209	$C_{17}H_{30}O_3$	CC1CC(C(C(C1CC=C(C)C)C)COC(=O)C)(C)O	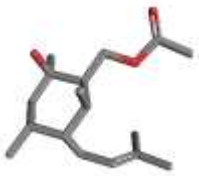

2.5 Experimental Design

Twenty male rats (160-180 g) were first randomized into two groups: control animals (Group 1, n=5) received 0.5 ml of distilled water, while the other group (BPH group, n=15) was given 6 mg/kg body weight of Testosterone Propionate (TP) (6mg/kg) subcutaneously once daily for 28 days after which the BPH group was divided into three groups of n=5: Group 2, no treatment; Group 3, treated with Finasteride 5 mg/kg BW; and Group 4, treated with 300 mg/kg BW aqueous extract of *Magaritaria discoidea* (AESBM) (Table 2). The treatments were administered orally for 28 days using an oro-gastric cannula.

Twelve hours after the final administration, the animals were subjected to overnight fasting with food and water withdrawn. Terminal body weights were measured, and anesthesia was induced through intraperitoneal injection of ketamine (40 mg/kg) combined with xylazine (4 mg/kg), following the protocol of (Wellington et al., 2013). Once deep anesthesia was confirmed, animals were humanely sacrificed. Blood samples were collected immediately via cardiac puncture into plain tubes, centrifuged at 3000 rpm for 15 minutes to obtain serum, which was then used for the analysis of serum biomarkers and testosterone concentration. The prostate glands were excised, weighed using an analytical balance (model DT 1000; 0.1–1000 g range), and preserved in two ways: some in 4 mL of freshly prepared 0.1 M phosphate-

buffered saline (PBS, pH 7.4) for biochemical assays, and others in 10% formal saline for histological analysis. The experimental design is displayed in Table 2.

Table 2: Experimental Design Table

Group	4 weeks (Induction)	4weeks (Treatment)	References
Control	0.5 ml Distilled water	0.5ml Distilled water	
BPH	Subcutaneous injection of testosterone-propionate 6 *mg/kg* body weight	No treatment	(Ogbu et al., 2020)
BPH + Finasteride	Subcutaneous injection of testosterone-propionate 6 *mg/kg* body weight	5mg/kg BW Finasteride	(Awarajih, 2015; Ogbu et al., 2020)
BPH + AESBM	Subcutaneous injection of testosterone-propionate 6 *mg/kg* body weight	300mg/kg BW AESBM	(Sofidiya et al., 2015; Ogbu et al., 2020)

2.6 Phosphate Buffer Preparation and Biochemical Assays

Before sacrifice, PBS (pH 7.4) was freshly prepared to preserve the testes and epididymis for biochemical analysis. This involved dissolving 7.162 g of sodium phosphate dibasic dodecahydrate ($Na_2HPO_4 \cdot 12H_2O$) in 200 mL of distilled water and 1.5603 g of sodium phosphate monobasic dihydrate ($NaH_2PO_4 \cdot 2H_2O$) in 100 mL of distilled water. The two solutions were mixed to create a 0.1 M buffer, and the pH was adjusted to 7.4 using drops of HCl or NaOH as needed (Fadanka et al., 2022).

All biochemical analyses were conducted under the supervision of certified medical laboratory scientists. Serum levels of prostate-specific antigen (PSA) (Catalogue Number: MB-2259A), testosterone (Catalogue Number: MB-2637A), and interleukin-6 (IL-6) (Catalogue Number: MB-2149A) were mearsured using rat-specific ELISA kits produced by Nanjing Mornmed Medical in Nanjing City, Jiangsu Province, China) based on sandwich and competitive ELISA methods, with absorbance read at 450 nm and concentrations calculated from standard curves (Ajayi et al., 2023).

To assess oxidative stress in prostate tissues, malondialdehyde (MDA) levels were measured using the TBARS method (Ajayi et al., 2023). Antioxidant enzyme activities—including superoxide dismutase (SOD), catalase (CAT), glutathione peroxidase (GPx), glutathione S-transferase (GST), and total thiols—were quantified using colorimetric techniques described (Hamed et al., 2022; Ajayi et al., 2024; Okeleji et al., 2025), with absorbance readings typically between 412 and 653 nm.

Inflammatory mediators such as tumor necrosis factor-alpha (TNF-α) (Catalogue Number: MB-5168A), interleukin-1 beta (IL-1β) (Catalogue Number: MB-5119A) were measured using ELISA kits (Nanjing Mornmed Medical in Nanjing City, Jiangsu Province, China)), and nitric oxide (NO) concentration was quantified via colorimetric method (Ajayi et al., 2023; Hamed et al., 2025). Caspase-3 (Catalogue Number: MB-3162A) activity indicative of apoptosis, was also measured using a sandwich ELISA kits (Nanjing Mornmed Medical in Nanjing City, Jiangsu Province, China).

2.7 Histological Assessment of the Prostate gland

The prostate tissues for histological evaluation were preserved in 10% formal saline and subsequently embedded in paraffin wax, after which sections measuring approximately 5–6 μm in thickness were prepared and stained with hematoxylin and eosin (H&E) for histopathological analysis; the sections were then observed under a light microscope and photomicrographs captured at ×100 magnification, while histopathological assessments were independently performed at the same magnification by two experts blinded to the study protocol (Bancroft & Gamble, 2008).

2.8 Statistical Analysis

Data were analyzed with GraphPad Prism version 10 (Windows), and outcomes were expressed as mean ± standards deviation. Comparative statistical evaluations within and across groups were performed using analysis of variance (ANOVA), followed by Tukey's post-hoc test, with intergroup the intergroup differences were considered statistically significant at $p < 0.05$.

3.0 Results

3.1 GC-MS Analysis of AESBM Extract

The GC-MS analysis of the aqueous extract of *Magaritaria discoidea* bark (AESBM) revealed eight distinct peaks on the total ion chromatogram. The major compounds eluted at retention times of 4.809 min, 13.501 min, and 15.120 min, contributing 25.79%, 35.94%, and 24.08%

of the total ion count, respectively (Figure 3). Key constituents identified included methyl benzoate, hexadecanoic acid methyl ester (methyl palmitate), and methyl stearate. Minor components such as undecane, a squalene-like derivative, photocitral B, and 2R-acetoxymethyl-trimethyl-cyclohexanol derivatives were also detected in lower proportions.

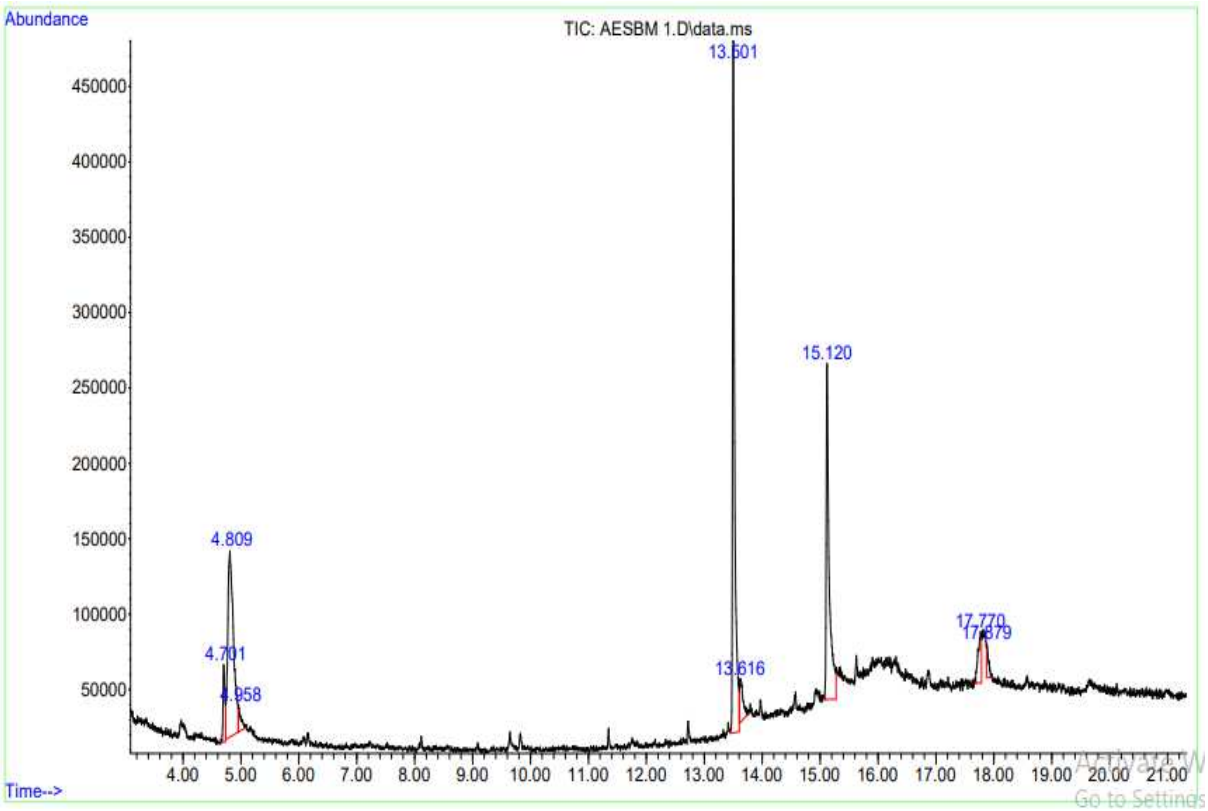

Figure 3: GC-MS Result showing the peaks and abundance of the ligands.

3.2 Insilico analysis

3.2.1 Molecular docking results

Molecular docking revealed that Lig 7 and Lig 8 showed the highest binding affinities to 5AR2 at -8.0 kcal/mol and -7.9 kcal/mol, respectively, surpassing Finasteride (-4.7 kcal/mol). Both ligands interacted predominantly with TYR91, PHE216, PHE219, CYS119, LEU224, and GLU57. Lig 3 demonstrated a binding affinity of -6.4 kcal/mol, forming a hydrogen bond with ASP164 and engaging ARG103, ARG168, ARG171, and ARG179. Lig 4 and Lig 5 had moderate affinities (-5.6 kcal/mol) and interacted with PHE118, PHE216, PHE219, and PHE223. Lig 1 and Lig 2 showed lower affinities (-5.0 and -5.4 kcal/mol) but still exceeded that of Finasteride, with interactions involving hydrophobic residues such as PHE118 and LEU224 (Table 3).

Table 3: *In-silico* elucidation of the select ligand and target (5AR2)

Ligand Number	Ligands	Binding Affinity (Kcal/Mol)	H-Bond Interaction	Hydrophobic/other interactions
Lig 0	Finsteride	-4.7		CYSS119, PHE118, TYR91, PHE216, PHE219, LEU224, PHE223, SER220, GLU57, GLY115
Lig 1	Undecane	-5.0		CYS119, PHE118, TYR91, PHE216, PHE219, LEU224, PHE223, SER220, GLU57, GLY115
Lig 2	Benzoic acid, methyl ester	-5.4		LYS35, TYR235, ARG168, ARG179, ARG171, SER177, GLY104, ARG103
Lig 3	Benzoyl isothiocyanate	-6.4	ASP164	LVS35, ARG168, TYR98, ARG103, GLY104, SER177, ARG179, LEU170, LEU167, TYR178, ARG172
Lig 4	Hexadecanoic acid, methyl ester	-5.6		PHE216, CYS119, GLY115, GLN56, PHE219, PHE223, PHE118, GLU197, TRP53, LEU224, PHE184, ARG94, ASN160, ASP164, ASN193, TYR98
Lig 5	Dodecanoic acid, 10-methyl-, methy l ester	-5.6	ARG94	PHE194, TRP53, LEU224, PHE223, PHE118, PHE219, ASN160, TYR33, GLU197, GLU57, PHE216, TYR91, TRP201
Lig 6	Methyl stearate	-5.3	TRP53	ARG227, TYR107, ALA49, ARG, 105, LYS35, HIS231, TYR33, GLY34,

			TYR178, GLY104, ASN102, LEU167, LEU170, ARG103, ARG171, ARG168, TYR98, ASP164
Lig 7	Oxirane, 2,2-dimethyl-3-(3,7,12,16,20-pentamethyl-3,7,11,15,19-heneicosapentaenyl)	-8.0	LEU224, SER220, PHE216, CYS119, GLU197, TLP201, TYR91, GLU57, PHE219, GLY115, TYR33, LEU20, SER31, ARG114, VAL27, LEU23, PHE223, PHE118, TLP53, ALA24
Lig 8	2R-Acetoxymethyl-1,3,5-trimethyl-4 c-(3-methyl-2-buten-1-yl)-1c-cyclo hexanol	-7.9	TRP201, TYR91, PHE216, SER220, PHE219, GLY115, HIS90, GLU57, ARG94, LEU224, GLU197, PHE194, ASN160, TRP53, PHE223, TYR33, SER31, PHE118

3.2.2 Drug Likeness analysis

All four ligands complied with Lipinski's rule and showed no major structural alerts. Lig 0 exhibited a balanced hydrophobicity (LogP 3.8145) and favorable molecular weight (372.54 Da), suggesting good oral bioavailability. Lig 3, with a lower molecular weight (163.20 Da) and LogP (1.9296), demonstrated higher hydrophilicity, supporting solubility and absorption. Lig 7 had the highest molecular weight (426.72 Da) and LogP (9.8162), indicating high hydrophobicity and potential low bioavailability (Table 4). Lig 8 showed moderate characteristics (MW 282.42 Da; LogP 3.5651), suggesting balanced permeability and solubility.

Table 4: Drug Likeness

S/N	Ligands	Molecular weight (k/ dalton)	LogP	No of H-bond donor	No of H-bond acceptor	No of violation	Lipinski alert
0	Lig 0	372.54	3.8145	2	2	0	NONE
1	Lig 3	163.201	1.9296	0	2	0	NONE
2	Lig 7	426.72	9.8162	0	1	0	NONE
3	Lig 8	282.42	3.5651	1	3	0	NONE

3.2.3 ADMET Analysis

All four compounds exhibited good absorption profiles, with high human intestinal absorption and acceptable Caco-2 permeability. Lig 3 showed the highest absorption potential. All compounds were capable of crossing the blood-brain barrier, with Lig 7 displaying the highest permeability (Table 5). In metabolic profiling, Lig 3 inhibited only CYP1A2, Lig 7 inhibited CYP3A4, Lig 8 showed no inhibition of major CYP450 enzymes, while Lig 0 inhibited CYP2C9. Lig 7 and Lig 8 demonstrated faster clearance rates than Lig 0 and Lig 3. Toxicity assessments indicated that all compounds were non-mutagenic and did not inhibit hERG1. However, Lig 0 showed hepatotoxicity, while Lig 3, 7, and 8 were not hepatotoxic

Table 5: ADMET profiling of Compound X and the 3 promising drug candidates

ADMET Parameters	**Compound X (standard)**	**Compound 3**	**Compound 7**	**Compound 8**
Absorption				
$CaCO_2$ permeability (log Papp in 10–6 cm/s)	1.269	1.653	1.176	1.386
HIA (% absorbed)	YES (93.742)	YES (95.069)	YES (91.045)	YES (94.243)
Distribution				
BBB permeability (log BB)	YES (-0.18)	YES (0.03)	YES (0.894)	YES (0.277)

Metabolism				
CYP450 1A2 inhibitor (Yes/No)	NO	YES	NO	NO
CYP450 2C19 inhibitor (Yes/No)	NO	NO	NO	NO
CYP450 2C9 inhibitor	YES	NO	NO	NO
CYP450 2D6 inhibitor (Yes/No)	NO	NO	NO	NO
CYP450 3A4 inhibitor (Yes/No**)**	NO	NO	YES	NO
Excretion				
Total clearance (log ml/min/kg)	0.38	0.119	1.396	1.265
Toxicity				
Ames toxicity (Yes/No)	NO	NO	NO	NO
hERG1 Inhibition (Yes/No)	NO	NO	NO	NO
Hepatotoxicity (Yes/No)	YES	NO	NO	NO

3.2.4 3D and 2D Analysis of Lead compounds and 5 Alpha reductase enzyme (52AR2)

The 3D and 2D analyses of the lead compounds binding to 5-alpha reductase type 2 (5AR2) using the crystal structure PDB: 7BW1 showed that all ligands docked successfully within the enzyme's active site. Finasteride formed stable hydrogen bonds with key residues GLN126, PHE118, and ASN193. Lig3 exhibited a similar binding pattern to Finasteride, with

comparable hydrogen bonds and hydrophobic contacts. Lig7 bound within the active site but had fewer or different hydrogen bonds, though it maintained hydrophobic interactions. Lig8 showed a balance of hydrogen bonding and hydrophobic interactions resembling Finasteride's profile (Figures. 4a-e). Overall, Lig3 had the closest interaction pattern to Finasteride, while Lig7 and Lig8 also demonstrated favorable binding, indicating their potential as 5AR2 inhibitors.

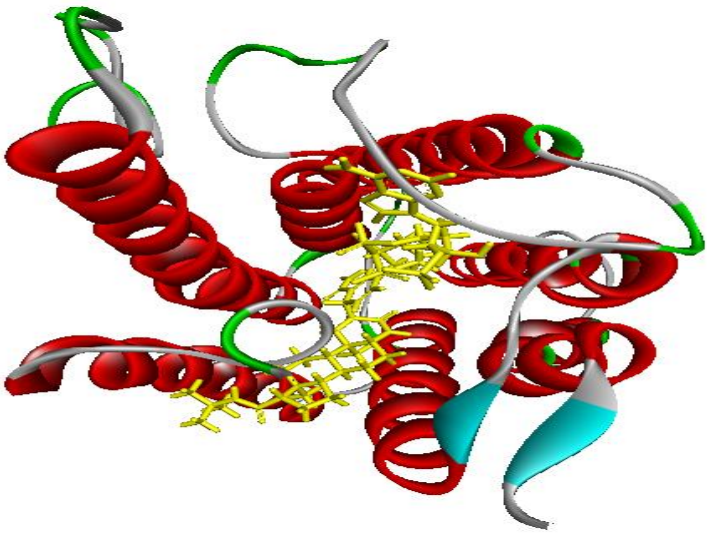

Figure 4a: 3D display of the interaction between select ligand and 5AR2 (PDB: 7BW1)

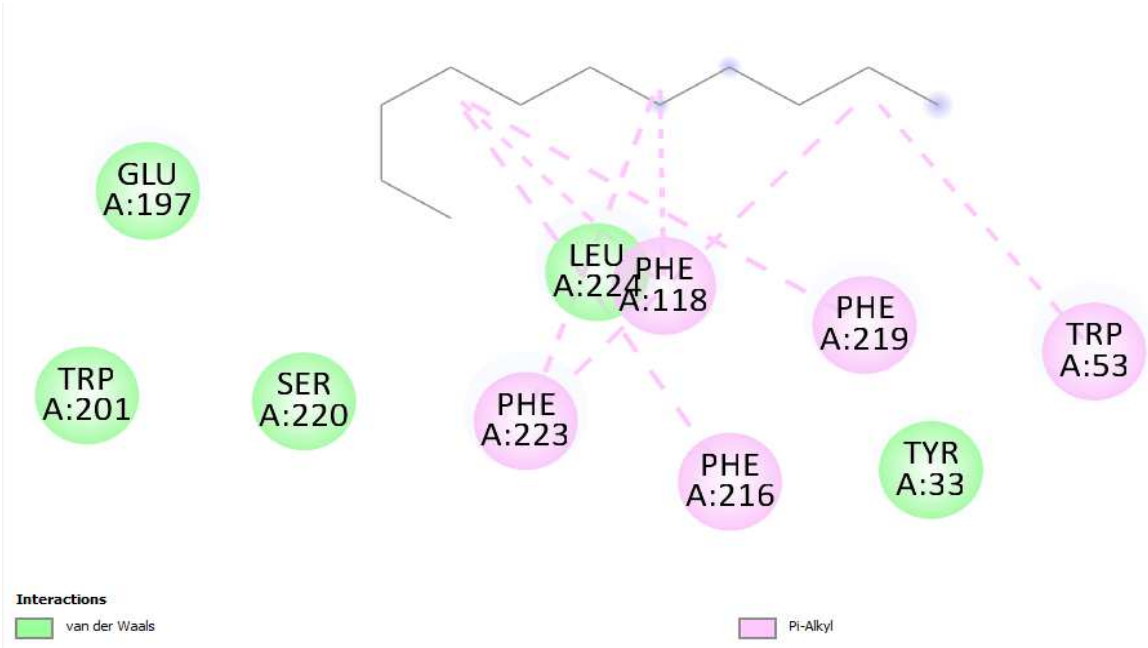

Figure 4b: 2D Display of the Finasteride and 5AR2 interaction.

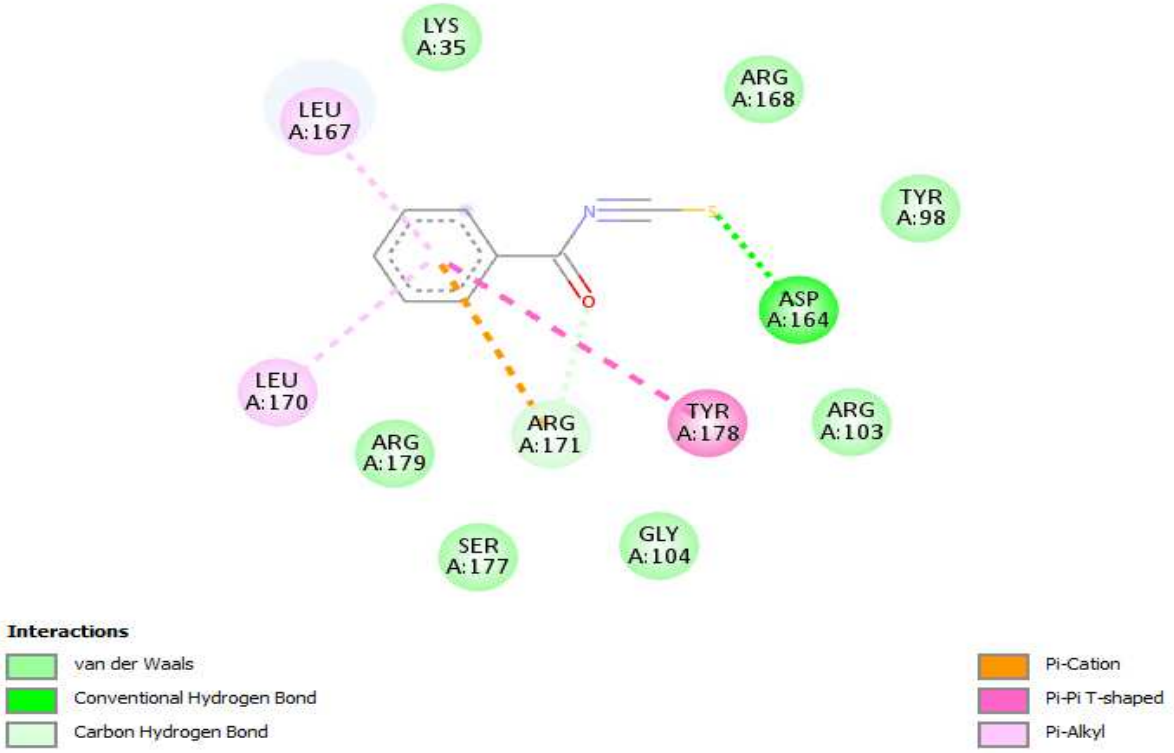

Figure 4c: 2D Display of the Lig3 and 5AR2 interaction.

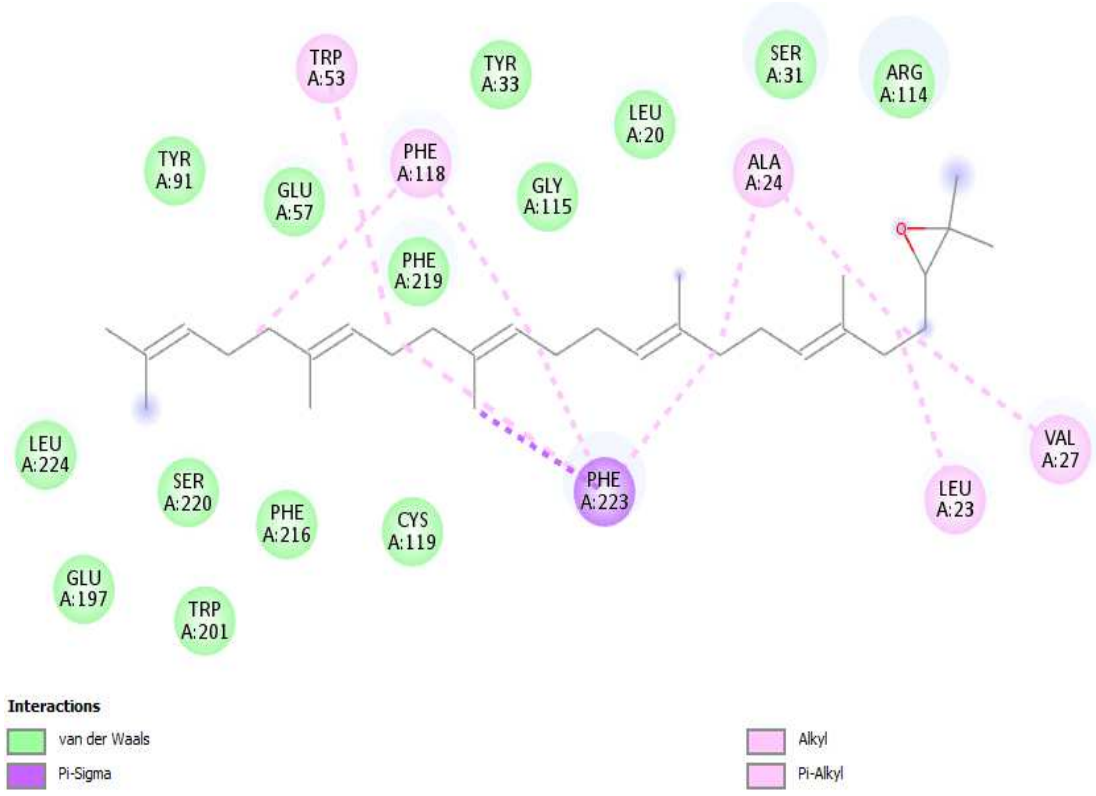

Figure 4d: 2D Display of the Lig7 and 5AR2 interaction.

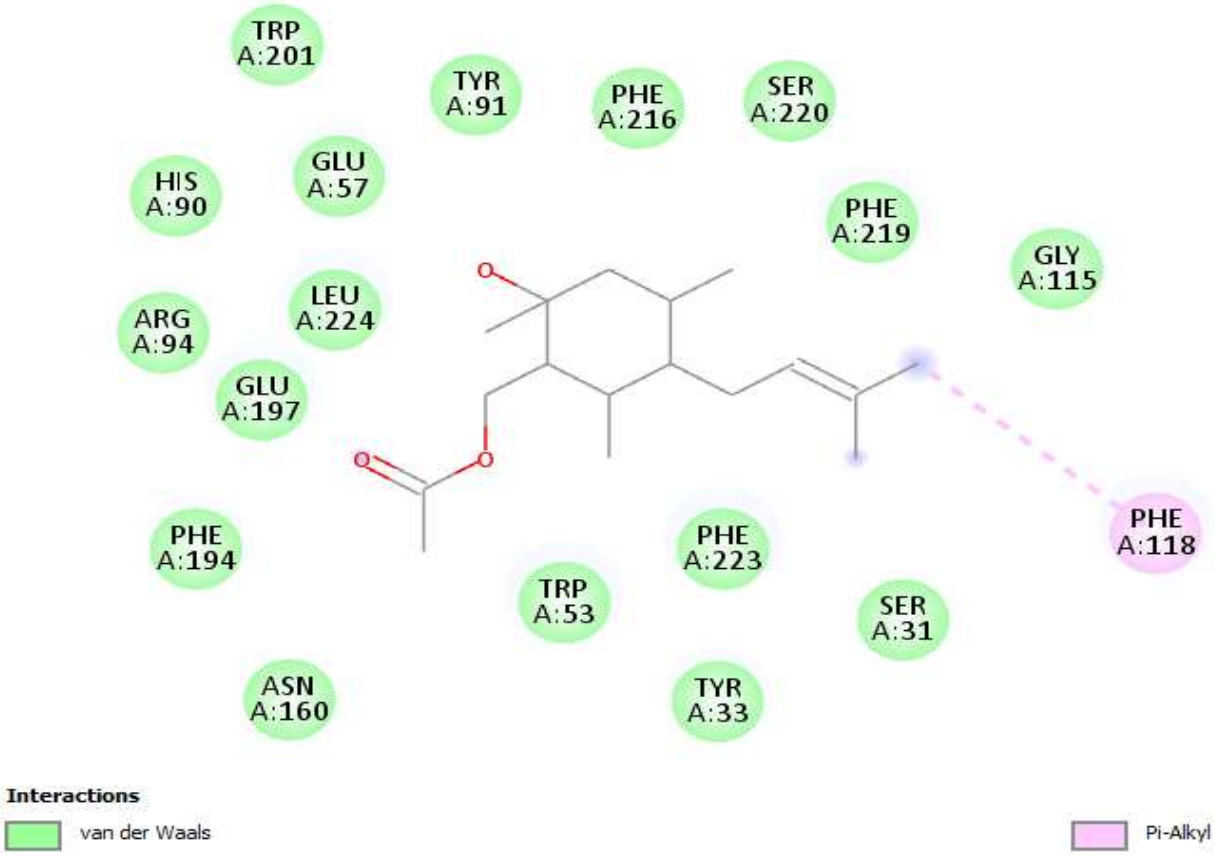

Figure 4e: 2D Display of the Lig8 and 5AR2 interaction.

3.3 Effects of AESBM on Body and Organ Weight in BPH induced Rats

There was no significant difference in the final body weight of the treated rats when compared (Figure 5a). The BPH group had a significantly increased prostate weight compared to the control. The treatment of BPH rats with AESBM resulted in a significant reduction ($p < 0.05$) in prostate weight when compared to the untreated BPH group, in line with finasteride treatment of rats with BPH (Figure 5b).

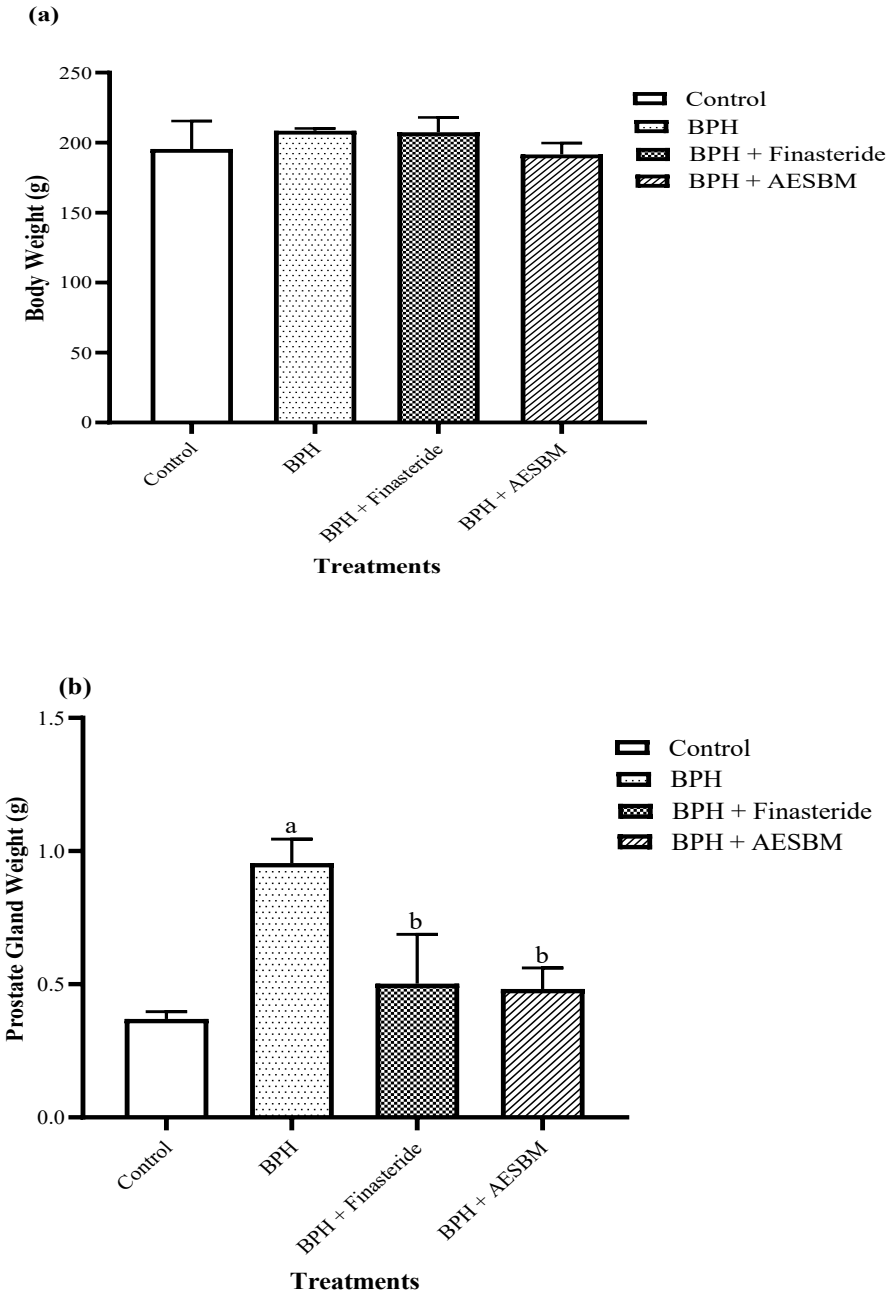

Figure 5: Effect of AESBM treatment on (a) final body weight (b) Prostate Weight in BPH-Induced Rats

Values are expressed as mean ± standard deviation (SD) for five replicate measurements. ***a*** *= significant (P < 0.05) compared with the control group;* ***b*** *= significant (P < 0.05) compared with the BPH group.*

3.4 Effects of AESBM on Serum PSA, Testosterone, and IL-6 Levels in BPH-Induced Rats

BPH induction resulted in a marked increase in serum PSA levels, testosterone concentration, and IL-6 compared to the control group ($p < 0.05$) (Figures 6a-c). Treatment with Finasteride and AESBM significantly lowered serum PSA levels, testosterone concentration, and IL-6 in BPH-induced rats compared to the untreated BPH group ($p < 0.05$) (Figures 6a-c). There was no significant difference in serum PSA levels, testosterone concentration, and IL-6 (Figures 6a-c) between the Finasteride-treated group and the AESBM-treated group, indicating that AESBM is equally effective in reducing PSA levels.

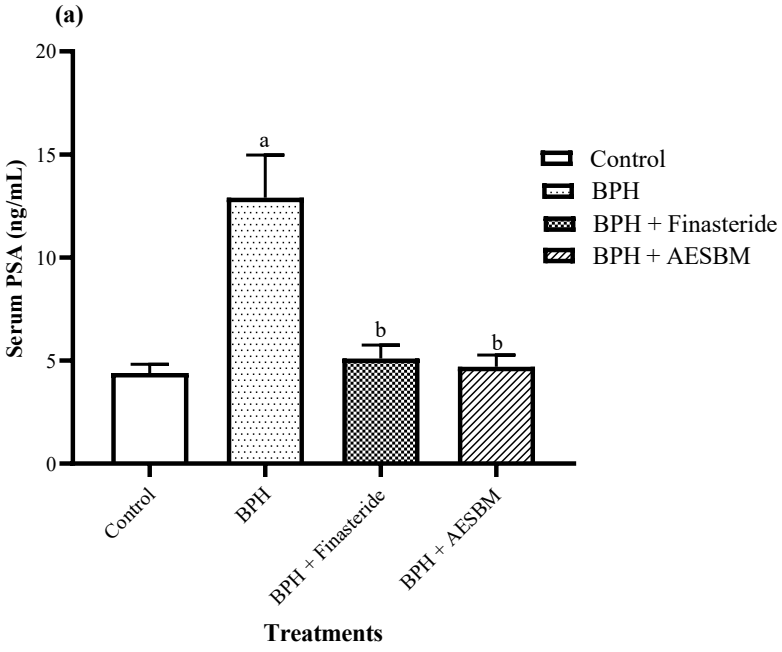

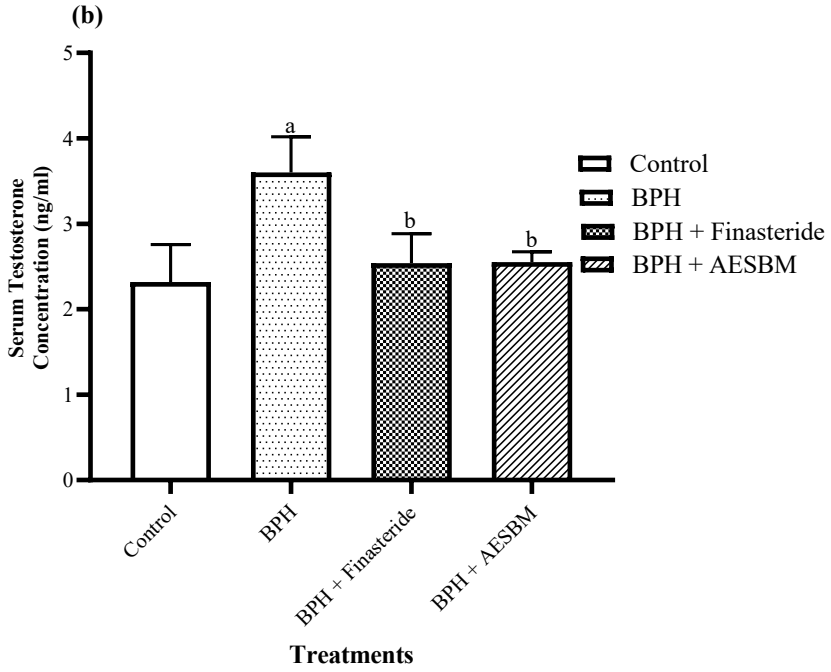
(b)
Serum Testosterone Concentration (ng/ml)
5
4
3
2
1
0
a
b
b
Control
BPH
BPH + Finasteride
BPH + AESBM
Treatments

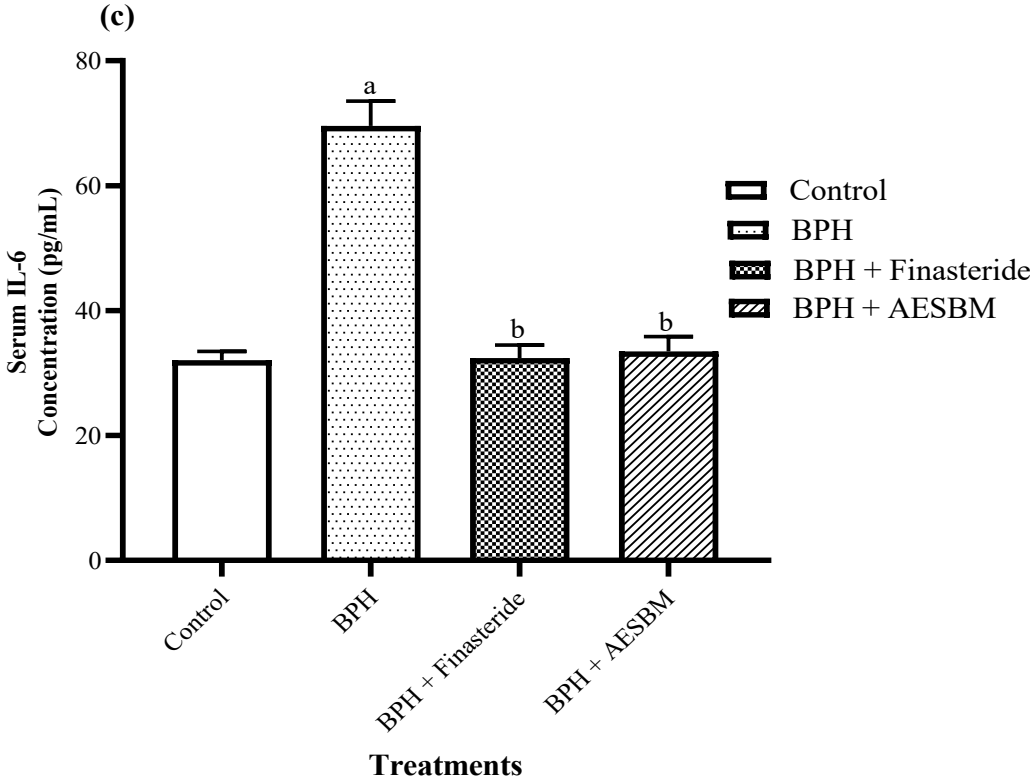

Figure 6: Effect of AESBM treatment on Serum (a) PSA (b) testosterone (c) IL-6 concentration in BPH-Induced Rats. *Values are presented as means of five replicate measurements ± SD. "a" denotes significant difference (P< 0.05) compared with the control group, while b indicates a significant difference (P< 0.05) compared with the BPH group.*

3.5 Effect of AESBM on Prostate Tissue Redox Markers

3.5.1 Lipid Peroxidation (MDA Levels)

The induction of BPH significantly elevated MDA levels ($p < 0.0001$) relative to the control group (Figure 7). Administration of Finasteride and AESBM resulted in a significant reduction in MDA levels compared with the untreated BPH group (Figure 7). However, prostate PSA concentrations did not differ significantly between the Finasteride-treated and AESBM-treated groups (Figure 7).

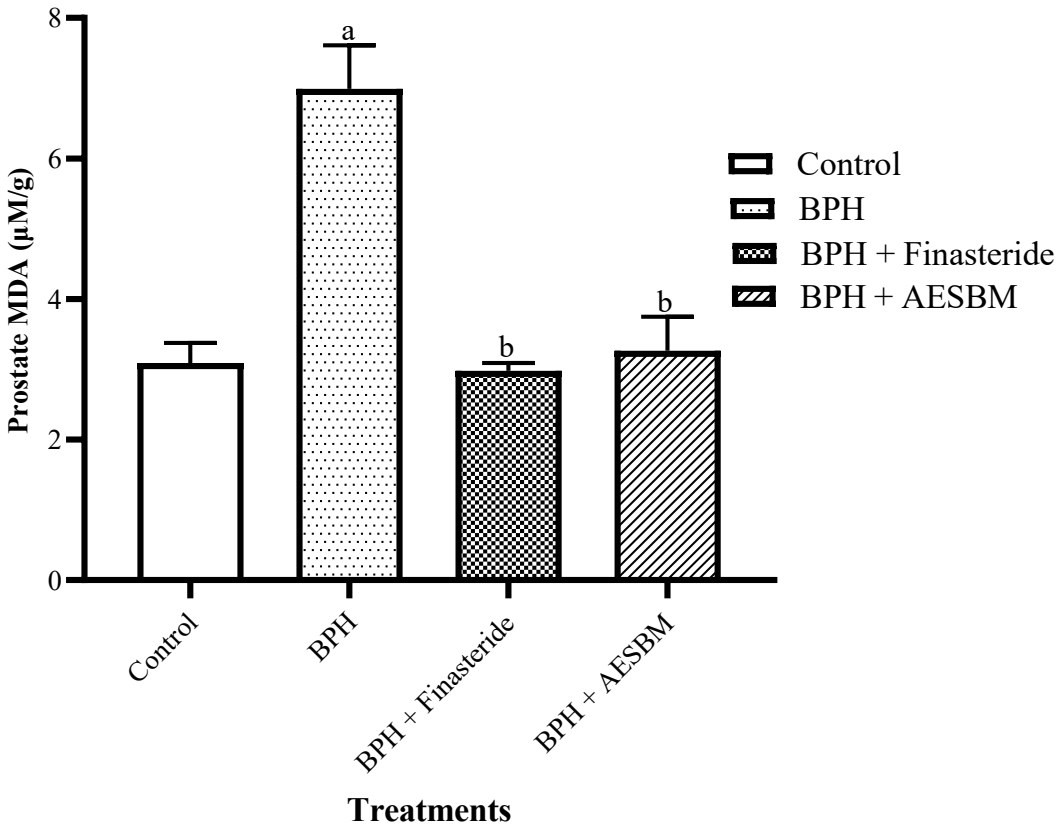

Figure 7: Effect of AESBM treatment on Prostate Tissue MDA in BPH-Induced Rats.
Values are presented as means of five replicate measurements ± SD. Statistical significance is indicated as follows: a denotes a significant difference (P< 0.05) compared with the control group, while b indicates a significant difference (P< 0.05) compared with the BPH group.

3.5.2 Prostate Tissue Antioxidant Status

The induction of BPH significantly ($p < 0.05$) reduced the prostate tissue antioxidant (SOD, catalase, GST, GPx, and total thiol) activities when compared to the control group. The administration of AESBM and Finasteride to BPH rats significantly ($p < 0.05$) increased prostate tissue SOD, catalase, GST, and total thiol activities (Table 6). The administration of AESBM to BPH rats had no significant effect when compared to the BPH group (Table 6).

Table 6: Prostate Tissues Antioxidants Status

Parameters	Control	BPH	BPH + Finasteride	BPH + AESBM
SOD (u/mg)	10.40 ± 1.342	2.30 ± 0.671^{a}	9.80 ± 1.643^{b}	10.40 ± 1.517^{b}
Catalase (u/mg)	7.07 ± 0.993	1.62 ± 0.556^{a}	7.46 ± 0.513^{b}	7.02 ± 0.992^{b}
GST (u/mg)	1.04 ± 0.11	0.83 ± 0.075^{a}	1.02 ± 0.072^{b}	0.96 ± 0.1016
GPx (u/mg)	0.17 ± 0.021	0.08 ± 0.007^{a}	0.15 ± 0.014^{b}	0.15 ± 0.007^{b}
Total Thiol (nmol/mg)	0.55 ± 0.121	0.40 ± 0.0027^{a}	$0.51 \pm 0.0450.045$	0.50 ± 0.0399

Values are presented as means of five replicate measurements ± SD. Statistical significance is indicated as follows: a denotes a significant difference (P< 0.05) compared with the control group, while b indicates a significant difference (P< 0.05) compared with the BPH group.

3.6 Effects of AESBM on Prostate Tissue Inflammatory markers

The induction of BPH resulted in a marked ($p < 0.05$) elevation of TNF-α, IL-1β, and NO concentrations in the prostatic tissue relative to the control group (Figures 8 a–c), whereas administration of AESBM to BPH-induced rats significantly ($p < 0.05$) attenuated TNF-α, IL-1β, and nitric oxide levels in the prostate when compared with the untreated BPH group (Figures 8 a–c).

(a)

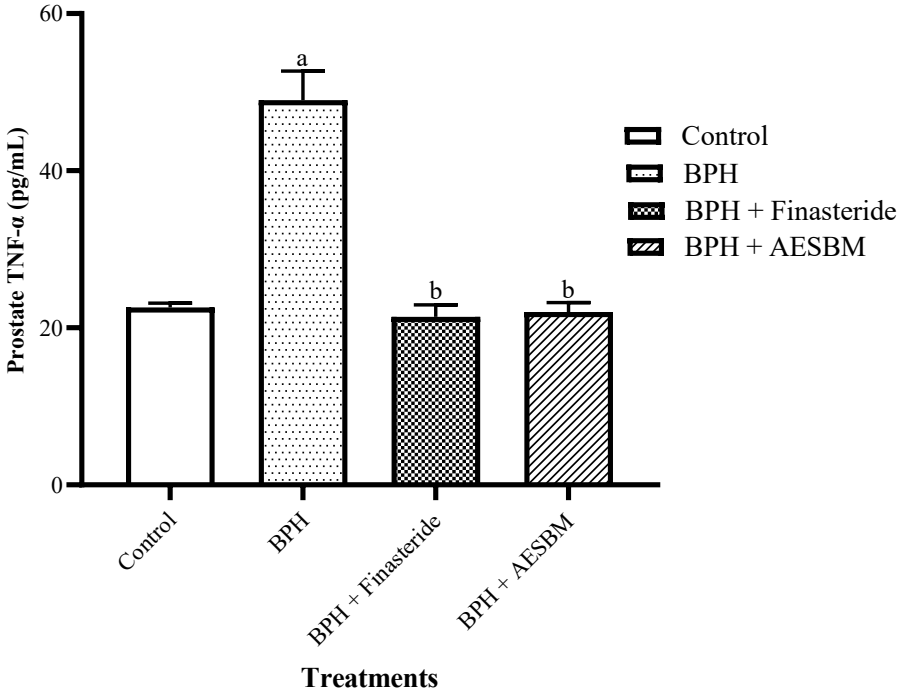
60
40
20
0
Prostate TNF-α (pg/mL)
a
b
b
Control
BPH
BPH + Finasteride
BPH + AESBM
Control
BPH
BPH + Finasteride
BPH + AESBM
Treatments

(b)

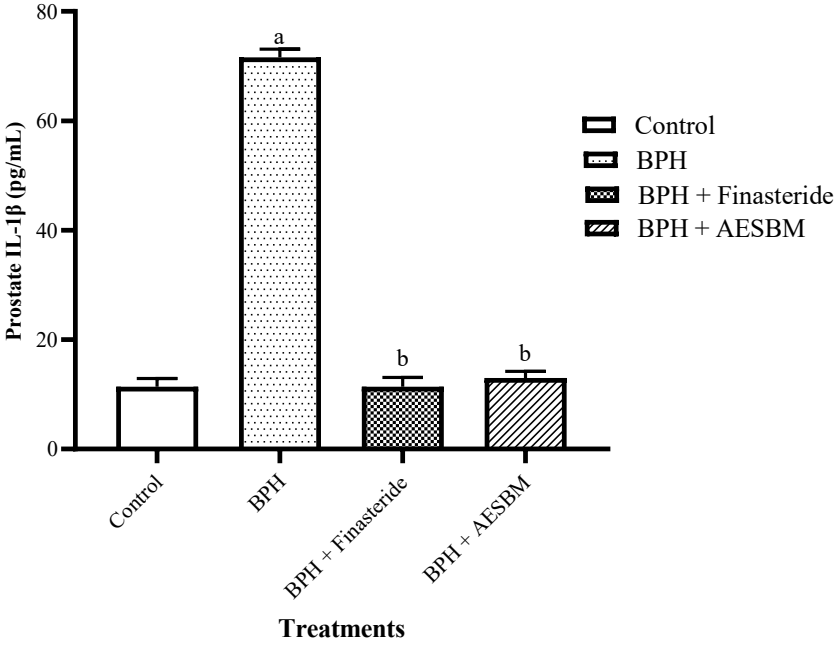
80
60
40
20
0
Prostate IL-1β (pg/mL)
a
b
b
Control
BPH
BPH + Finasteride
BPH + AESBM
Control
BPH
BPH + Finasteride
BPH + AESBM
Treatments

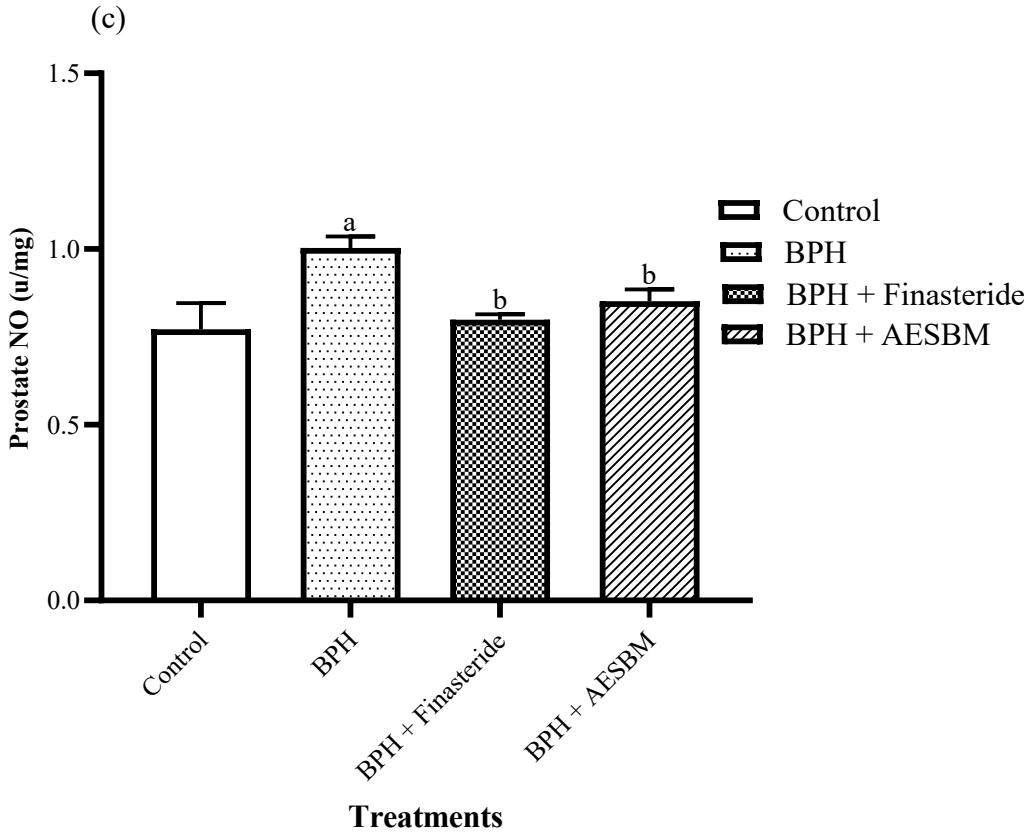

Figure 8: Effect of AESBM treatment on Prostate Tissue (a) TNF-α (b) IL-1β (c) NO activities in BPH-Induced Rats. *Values are presented as means of five replicate measurements ± SD. Statistical significance is denoted as follows: a indicates a significant (P< 0.05) increase compared with the control group, while b represents a significant (P< 0.05) decrease compared with the BPH group.*

3.7 Effects of AESBM on Prostate Tissue Apoptotic marker

The caspase-3 levels in the BPH ats were markedly elevated ($p < 0.05$) relative to the control group (Figure 9). The administration of AESBM to BPH rats significantly ($p < 0.05$) reduced caspase-3 levels in a pattern similar to finasteride treatment (Figure 9).

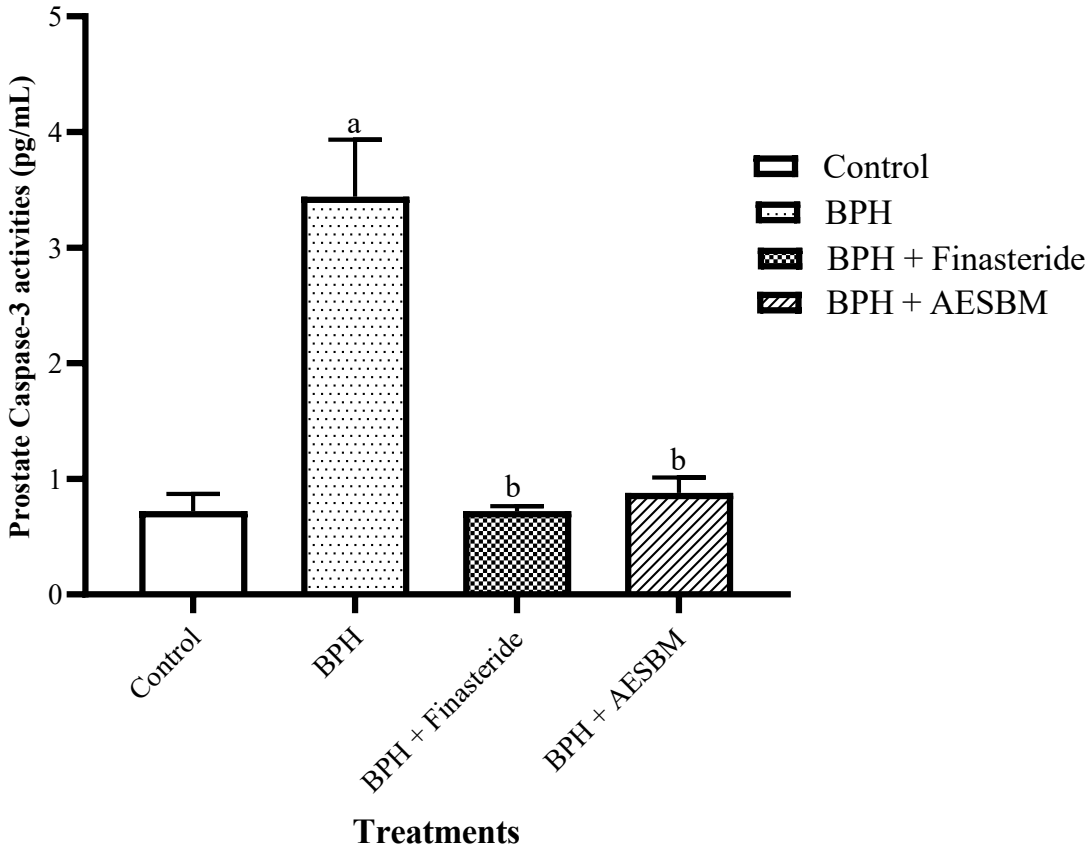

Figure 9: Effect of AESBM treatment on Prostate Tissue Caspase 3 in BPH-Induced Rats
The values are presented as means of five replicate measurements ± SD. Statistical significance is denoted as follows: a indicates a significant ($P < 0.05$) increase compared with the control group, while b represents a significant ($P < 0.05$) decrease compared with the BPH group.

3.8 Histological analysis of the prostate

The histological examination of the prostate, shown in Plate 1, revealed significant differences between the groups. In the control rats, the prostate structure was well-preserved, with intact tubuloalveolar glands, corpora amylacea, and epithelial cells. In contrast, the BPH group showed notable pathological changes, including thickened epithelial cell layers, glandular hyperplasia, enlarged luminal areas, inflammatory cell infiltration, and prominent fibromuscular stroma, indicating prostate enlargement and inflammation.

Treatment with Finasteride restored the prostate architecture to near normal, resembling the control group. Similarly, rats treated with AESBM at 300 mg/kg demonstrated progressive structural recovery. These groups showed normalized epithelial layers, reduced inflammation,

and restored glandular volume and luminal space, comparable to Finasteride. Overall, AESBM treatment effectively reversed BPH-induced histological changes.

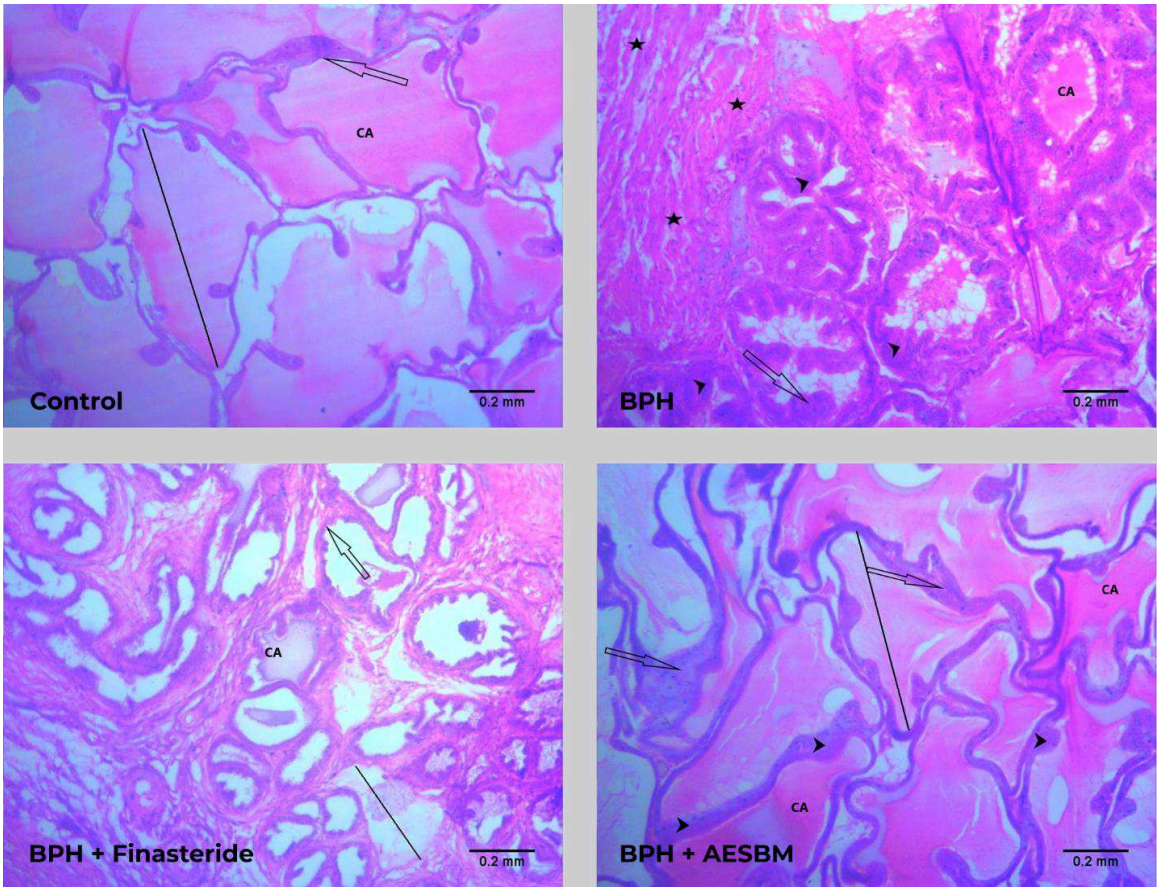

Plate 1: Photomicrograph of the histoarchiteocture of the prostate tissue, H&E (X 100).

The tubuloaveolar (straight line), corpora amylacea (CA) and epithelial-cell (arrow), glandular epithelial cells (arrow), proliferating glands (arrowhead), fibromuscular stroma (star).

4.0 Discussion

The prostate, an accessory gland of the male reproductive system, produces the majority of seminal fluid during ejaculation by secreting a whitish, watery prostatic fluid enriched with calcium, citrate, phosphate ions, a coagulating enzyme, and profibrinolysin, which collectively provide nutrients and establish a favorable environment that enhances sperm motility and survival within the female reproductive tract (Barrett et al., 2019). The prostate gland is androgen-dependent, responding to serum testosterone levels, which consequently regulate its function and anatomy (Mononen et al., 2002; Tika et al., 2019). In aging men, the prostate may become enlarged due to various reasons such as inflammation, vascular aging, and testosterone decline (Corona et al., 2017; Phua, 2021).

The decreasing levels of testosterone alongside prostate enlargement appear paradoxical. However, the "saturation hypothesis" suggests that the prostate's sensitivity to androgens is limited beyond a certain threshold, explaining why BPH progresses despite declining testosterone levels (Morgentaler & Traish, 2009). Studies show a sigmoidal relationship between testosterone and PSA, which plateaus at 8 nmol/L, while intraprostatic DHT levels remain stable regardless of circulating testosterone (Rastrelli et al., 2013; Van Der Sluis et al., 2012). Age-related testosterone decline (2–3% yearly) promotes prostate enlargement via androgen receptor-mediated transcription of growth factors such as IGF-1, EGF, and FGF (Rastrelli et al., 2013). Evidence also shows that, despite testosterone decline, testosterone can be converted to 5α-dihydrotestosterone (DHT) in the presence of 5α-reductase, which stimulates the transcription of growth factors, thereby promoting epithelial and stromal proliferation (Choi et al., 2021). Testosterone can also be converted to estradiol-17β via aromatase, and the estrogen-to-testosterone (E/T) ratio has been implicated in BPH pathogenesis (Zhou et al., 2009). Elevated estrogen levels in aging men may enhance androgen receptor sensitivity, further contributing to prostate enlargement (Zhou et al., 2009; Nicholson et al., 2012; Li et al., 2018).

Benign prostatic hyperplasia (BPH), a common urological disorder often result in lower urinary tract symptoms (LUTS), characterized by impaired urinary flow and storage, leading to a compromised immune system due to prostatic proliferation obstructing the bladder outlet (Lim, 2017; Shapiro & Lepor, 1995). In prolonged cases, the reproductive system may also be compromised, causing infertility (Kayode et al., 2020). Although surgical procedures and medications like Finasteride are commonly used for managing BPH, these treatments often result in undesirable side effects such as retrograde ejaculation, low libido, and incontinence. This study investigated the antiproliferative, anti-inflammatory, antioxidant, and anti-apoptotic effects of the aqueous extract of *Margaritaria discoidea* bark (AESBM) in a rat model of BPH.

GC-MS analysis of AESBM revealed eight prominent peaks, with methyl benzoate, methyl palmitate (hexadecanoic acid, methyl ester), and methyl stearate as the most abundant constituents, collectively accounting for 85.81% of the total ion count. These compounds are well-recognized for their anti-inflammatory, antimicrobial, and antioxidant properties (Obiri et al., 2014). Notably, methyl palmitate and methyl stearate—long-chain fatty acid esters—are known to modulate lipid metabolism and inflammatory responses (Mjabri et al., 1992). The presence of undecane and squalene-like derivatives suggests additional roles in enhancing

lipophilic compound absorption and improving membrane fluidity, thus facilitating interactions with intracellular targets such as 5α-reductase type 2 (5AR2) (El-Maradny, 2012). The chemical complexity of AESBM implies potential synergistic effects among its constituents, contributing collectively to its pharmacological activity.

Molecular docking studies revealed that AESBM-derived phytocompounds—particularly Lig 7 and Lig 8—exhibited strong inhibitory effects on 5AR2, surpassing finasteride in binding affinity. These compounds formed stable interactions with hydrophobic residues in the enzyme's active site. Lig 3 exhibited a different binding mode, dominated by hydrogen bonding and electrostatic interactions, but still showed considerable affinity. Other ligands (Lig 1, Lig 2, Lig 4, and Lig 5) also demonstrated moderate to strong binding affinities, supporting the therapeutic potential of AESBM's diverse phytochemical constituents.

Pharmacokinetic profiling using the pkCSM web server (Pires et al., 2015; Yang et al., 2019) showed that all ligands met basic drug-likeness criteria. Lig 3 stood out for its favorable characteristics, including low molecular weight, high solubility, and optimal ADMET parameters. Lig 8 also exhibited a balanced pharmacokinetic profile. However, despite Lig 7's high potency, its poor solubility due to high lipophilicity suggests the need for formulation optimization. Overall, Lig 3 emerged as the safest candidate, with excellent absorption, minimal cytochrome inhibition, and no predicted toxicity. Lig 8 also demonstrated favorable metabolic and safety profiles, whereas Lig 7 raised concerns due to its enzyme inhibition and clearance rates. Thus, Lig 3 and Lig 8 represent the most promising candidates, though structural or formulation adjustments may enhance Lig 7's viability.

BPH induction using testosterone propionate was confirmed by a significant increase in prostate weight and PSA levels. Prior studies have identified prostate weight gain as a hallmark of BPH progression, reflecting stromal and epithelial cell hypertrophy (Veeresh Babu et al., 2010; Li et al., 2018). In this study, AESBM treatment significantly reduced prostate weight compared to the untreated BPH group. While body weight remained largely unchanged, the prostate hypertrophy observed typifies BPH pathology (Ogheneochuko et al., 2024). The reduction in prostate weight following AESBM treatment (300 mg/kg) may be attributed to its antiproliferative effects, likely mediated through antioxidant and anti-inflammatory mechanisms (Johnson-Ajinwo et al., 2015; Ekuadzi et al., 2018; Gwedela et al., 2022).

Testosterone propionate administration significantly elevated PSA levels, consistent with earlier reports (Ogbu et al., 2020), thereby confirming successful BPH induction. (Aigbe et al., 2022) also reported that larger benign prostates are associated with elevated PSA levels, emphasizing the need to consider BPH—not just malignancy—as a potential cause of PSA elevation. The increased prostate weight and PSA levels observed in rats treated with testosterone propionate confirm BPH induction, consistent with previous findings (Ogbu et al., 2020), which attributed these effects to increased stromal and epithelial cell proliferation—a hallmark of BPH. Treatment with AESBM and finasteride resulted in marked reductions in PSA levels and prostate weight, highlighting the anti-proliferative effects of AESBM.

High circulating testosterone levels stimulate 5α-reductase, converting testosterone into DHT—a key factor in BPH development and progression (Kayode et al., 2020). Finasteride (5 mg/kg), a 5α-reductase type 2 inhibitor, blocks this conversion, thereby reducing PSA levels and prostate volume (Fahmy & Hess, 2024). This study confirms that BPH induction led to significant increases in serum PSA and testosterone levels. However, treatment with AESBM (300 mg/kg) and finasteride effectively normalized both parameters. Additionally, BPH induction elevated interleukin-6 (IL-6), a pro-inflammatory cytokine, consistent with earlier findings (Obiri et al., 2014). Treatment with AESBM and finasteride significantly reduced IL-6 levels, indicating a strong anti-inflammatory response.

BPH induction also led to elevated malondialdehyde (MDA) levels which is a marker of lipid peroxidation, along with reduced antioxidant enzyme activity (SOD, GPx), aligning with earlier studies (Ekuadzi et al., 2018; Ogbu et al., 2020). AESBM treatment (300 mg/kg) restored redox balance by significantly lowering MDA activity and enhancing SOD and GPx concentration. These antioxidant effects likely result from the polyphenolic and flavonoid content of *Margaritaria discoidea*, known for scavenging reactive oxygen species (Obiri et al., 2014; Johnson-Ajinwo et al., 2015). The GC-MS-identified compounds (methyl benzoate, methyl palmitate, methyl stearate) further support these observations due to their documented antioxidant and anti-inflammatory activity (Mjabri et al., 1992; El-Maradny, 2012; Obiri et al., 2014).

Cytokine profiling showed that BPH induction significantly elevated TNF-α and IL-1β levels in prostatic tissue, reflecting systemic inflammation linked to hormonal imbalance and tissue remodeling (Obiri et al., 2014). AESBM (300 mg/kg) significantly downregulated these pro-inflammatory cytokines, highlighting its potent anti-inflammatory activity—possibly through

NF-κB pathway inhibition (Johnson-Ajinwo et al., 2015). Notably, cytokine levels in AESBM-treated rats closely matched those of the finasteride group, reinforcing the extract's therapeutic relevance.

Apoptotic dysregulation was evident in the BPH control group, as shown by elevated caspase-3 levels (Huang et al., 2022), indicating inflammation- and oxidative stress-induced cell death. Previous studies have shown that *Margaritaria discoidea* extracts exert cytotoxic effects, especially against ovarian cancer cells, due to compounds like gallic acid and securinine (Johnson-Ajinwo et al., 2015). AESBM treatment (300 mg/kg) significantly reduced caspase-3 activity, suggesting preservation of cellular integrity in prostate tissue.

Histopathological findings further validated the biochemical outcomes. Prostate sections from BPH-induced rats showed glandular hyperplasia, epithelial thickening, and fibromuscular stromal proliferation—classic features of BPH (Li et al., 2018). Treatment with AESBM (300 mg/kg) restored prostate architecture to near-normal, comparable to the finasteride-treated group, with normalized luminal spaces, reduced inflammation, and restored glandular structure.

AESBM (300 mg/kg) provides multifaceted protection against BPH through antioxidant, anti-inflammatory, and anti-apoptotic mechanisms. Improvements observed across molecular, biochemical, and histological parameters highlight its therapeutic potential, comparable in many respects to finasteride. The phytochemical diversity of *Margaritaria discoidea* likely contributes synergistically to modulate the complex pathophysiology of BPH. Figure 10 is a schematic of the contribution to knowledge of this work.

5. Conclusion

This study demonstrates the potential of *Margaritaria discoidea* aqueous extract (AESBM) as a promising therapeutic agent for benign prostatic hyperplasia (BPH) management, revealing anti-proliferative activity mediated via antioxidant, anti-inflammatory, and anti-apoptotic mechanisms. The findings provide a strong preclinical basis for further research, including clinical trials, to explore its safety, efficacy, and potential as a natural alternative or adjunct therapy for BPH treatment.

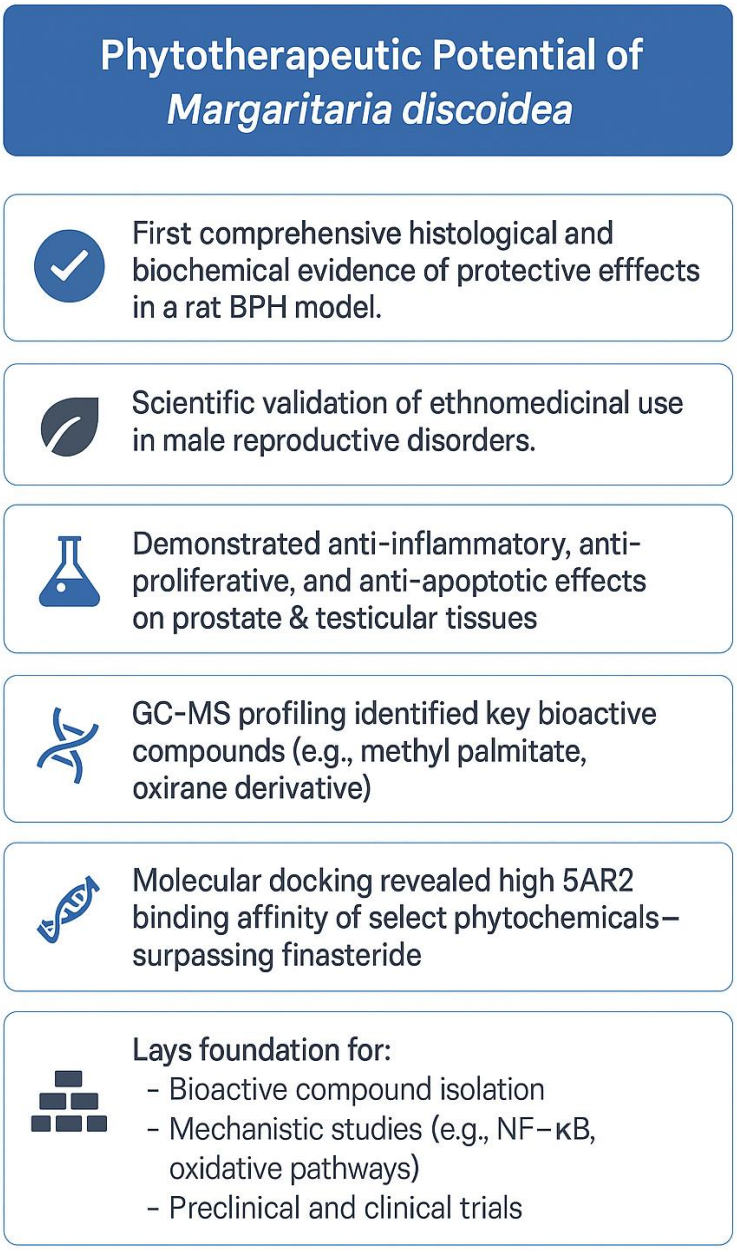

Figure 10: A schematic of the contribution to knowledge

Declarations

Funding: This research did not receive any specific grant from any funding agency in the public, commercial, or not-for-profit sectors.

Conflict of Interest: The authors affirm that they possess no known financial interests or personal affiliations that could have affected the objectivity or outcomes of the research presented in this manuscript. **Ethical Approval**: The Research Ethics Review Committee of the Faculty of Basic Medical Sciences, Ladoke Akintola University of Technology (LAUTECH), Oyo State, Nigeria, granted ethical clearance for this investigation (Approval No.: ERCFBMSLAUTECH:089/01/2025), and all experimental protocols involving animals were conducted in strict compliance with institutional and internationally accepted standards governing the care and utilization of laboratory animals.

Clinical Trial Registration: Not applicable (the investigation did not include human subjects or clinical trial procedures).

Consent to Publish: Not applicable (no human data or images are included).

Availability of data and materials: data sets that are used for this work are publicly available.

Author Contributions: **B.O.A.**: Conceptualization, Methodology, Investigation, Writing – Original Draft. **O.D.T.**: Formal Analysis, Data Curation, Writing – Review & Editing. **M.A.H.**: Methodology, Validation, Resources. **O.P.A.**: Investigation, Visualization. **A.F.A.**: Supervision, Project Administration, Writing – Review & Editing.

Acknowledgments: Nil.

References

Agbabiaka, T. B., Pittler, M. H., Wider, B., & Ernst, E. (2009). Serenoa repens (saw palmetto): A systematic review of adverse events. *Drug Safety*, *32*(8), 637–647. https://doi.org/10.2165/00002018-200932080-00003

Agilent. (2019). *The Source of New Possibilities*.

Aigbe, E., Irekpita, E., Ogbetere, F. E., & Alili, U. I. (2022). Correlation between prostate volume and prostate-specific antigen in Nigerian men with symptomatic histologically-diagnosed benign prostatic hyperplasia. *Nigerian Journal of Clinical Practice*, *25*(9), 1523–1528.

Ajayi, A. F., Ogundipe, O. O., Hamed, M. A., & Oluwole, D. T. (2024). Skoochies and component substances induced testicular damage and impaired sperm function via

increased generation of reactive oxygen species and impairment of the glutathione system in rats. *F&S Science*, *5*(4), 318-330.

Ajayi, A. F., Onaolapo, M. C., Omole, A. I., Adeyemi, W. J., & Oluwole, D. T. (2023). Mechanism associated with changes in male reproductive functions during ageing process. *Experimental Gerontology*, *179*, 112232.

Awarajih. (2015). *testosterpone propionaet Awarajih et al., 2015—Google Search*. https://www.google.com/search?q=testosterpone+propionaet+Awarajih+et+al.%2C+2015&rlz=1C1GCEU_enNG1162NG1162&oq=testosterpone+propionaet+Awarajih+et+al.%2C+2015&gs_lcrp=EgZjaHJvbWUyBggAEEUYOTIKCAEQABiABBiiBDIKCAIQABiABBiiBDIHCAMQABjvBTIHCAQQABjvBTIHCAUQABjvBdIBCDc1MjdqMGo0qAIAsAIB&sourceid=chrome&ie=UTF-8

Bancroft, J. D., & Gamble, M. (2008). *Theory and practice of histological techniques*. Elsevier health sciences. https://books.google.com/books?hl=en&lr=&id=Dhn2KispfdQC&oi=fnd&pg=PR13&dq=Bancroft,+J.+D.,+%26+Gamble,+M.+(2008).+Theory+and+Practice+of+Histological+Techniques+(6th+ed.).+Churchill+Livingstone/Elsevier.&ots=JCmHkATuB9&sig=3KhtyKP1NLZb2nqxPBa_HRGdkeI

Barrett, K. E., Barman, S. M., Yuan, J. X.-J., & Brooks, H. (2019). *Ganong's review of medical physiology, 26e* (26th ed.). McGraw-Hill Education LLC.

Choi, D., Kim, J., An, J., Hong, S., Song, Y., & Kong, H. (2021). Amelioration of Benign Prostatic Hyperplasia by Costunolide and Dehydrocostus Lactone in Wistar Rats. *The World Journal of Men's Health*, *39*(2), 315–323. https://doi.org/10.5534/wjmh.190053

Corona, G., Tirabassi, G., Santi, D., Maseroli, E., Gacci, M., Dicuio, M., Sforza, A., Mannucci, E., & Maggi, M. (2017). Sexual dysfunction in subjects treated with inhibitors of 5α-

reductase for benign prostatic hyperplasia: A comprehensive review and meta-analysis. *Andrology*, *5*(4), 671–678. https://doi.org/10.1111/andr.12353

Couch, G. S., Hendrix, D. K., & Ferrin, T. E. (2006). Nucleic acid visualization with UCSF Chimera. *Nucleic Acids Research*, *34*(4), e29–e29.

Dagar, R., Gautam, A., Priscilla, K., Sharma, V., Gupta, P., & Kumar, R. (2024). Sample Preparation from Plant Tissue for Gas Chromatography–Mass Spectrometry (GC-MS)we. In F. Maghuly (Ed.), *Plant Functional Genomics* (Vol. 2788, pp. 19–37). Springer US. https://doi.org/10.1007/978-1-0716-3782-1_2

Ekuadzi, E., Biney, R. P., Benneh, C. K., Osei Amankwaa, B., & Jato, J. (2018). Antiinflammatory properties of betulinic acid and xylopic acid in the carrageenan-induced pleurisy model of lung inflammation in mice. *Phytotherapy Research: PTR*, *32*(3), 480–487. https://doi.org/10.1002/ptr.5993

El-Maradny, A. (2012). Identification of Fatty Acid Methyl Esters, Long Chain Aldehydes and Free Fatty Acids in a Sponge Chalinula saudensis along the coast of Jeddah, Saudi Arabia. *J. Chem. Soc. Pak*, *34*(3). https://www.researchgate.net/profile/Amr-Maradny-2/publication/287607620_Identification_of_fatty_acid_methyl_esters_long_chain_aldehydes_and_free_fatty_acids_in_a_sponge_chalinula_saudensis_along_the_coast_of_Jeddah_Saudi_Arabia/links/56b05ad308ae9ea7c3adfb1e/Identification-of-fatty-acid-methyl-esters-long-chain-aldehydes-and-free-fatty-acids-in-a-sponge-chalinula-saudensis-along-the-coast-of-Jeddah-Saudi-Arabia.pdf?_sg%5B0%5D=started_experiment_milestone&origin=journalDetail&_rtd=e30%3D

Fadanka, S., Minette, S., & Mowoh, N. (2022). *Preparation of PBS Solution*. https://www.protocols.io/view/preparation-of-pbs-solution-b85dry26.html

Gasteiger, J., & Marsili, M. (1980). Iterative partial equalization of orbital electronegativity—A rapid access to atomic charges. *Tetrahedron*, *36*(22), 3219–3228.

Gravas, S., Gacci, M., Gratzke, C., Herrmann, T. R. W., Karavitakis, M., Kyriazis, I., Malde, S., Mamoulakis, C., Rieken, M., Sakalis, V. I., Schouten, N., Speakman, M. J., Tikkinen, K. A. O., & Cornu, J.-N. (2023). Summary Paper on the 2023 European Association of Urology Guidelines on the Management of Non-neurogenic Male Lower Urinary Tract Symptoms. *European Urology*, *84*(2), 207–222. https://doi.org/10.1016/j.eururo.2023.04.008

Gwedela, M. N. V., Terai, H., Lampiao, F., Matsunami, K., & Aizawa, H. (2022). Anti-seizure effects of medicinal plants in Malawi on pentylenetetrazole-induced seizures in zebrafish larvae. *Journal of Ethnopharmacology*, *284*, 114763. https://doi.org/10.1016/j.jep.2021.114763.

Hamed, M. A., Akhigbe, T. M., Akhigbe, R. E., Aremu, A. O., Oyedokun, P. A., Gbadamosi, J. A., ... & Ajayi, A. F. (2022). Glutamine restores testicular glutathione-dependent antioxidant defense and upregulates NO/cGMP signaling in sleep deprivation-induced reproductive dysfunction in rats. *Biomedicine & Pharmacotherapy*, *148*, 112765.

Hamed, M. A., Akhigbe, R. E., Ekundina, V. O., & Oluwole, D. T. (2025). Promethazine induces testicular and epididymal toxicity via the upregulation of xanthine oxidase/uric acid-mediated oxidative stress signaling. *Comparative Clinical Pathology*, *34*(2), 215-230.

Huang, G., He, X., Xue, Z., Long, Y., Liu, J., Cai, J., Tang, P., Han, B., Shen, B., Huang, R., & Yan, J. (2022). Rauwolfia vomitoria extract suppresses benign prostatic hyperplasia by inducing autophagic apoptosis through endoplasmic reticulum stress. *BMC Complementary Medicine and Therapies*, *22*(1), 125. https://doi.org/10.1186/s12906-022-03610-4

Johnson-Ajinwo, O. R., Richardson, A., & Li, W.-W. (2015). Cytotoxic effects of stem bark extracts and pure compounds from Margaritaria discoidea on human ovarian cancer cell lines. *Phytomedicine: International Journal of Phytotherapy and Phytopharmacology*, *22*(1), 1–4. https://doi.org/10.1016/j.phymed.2014.09.008

Kayode, O. T., Rotimi, D. E., Kayode, A. A., Olaolu, T. D., & Adeyemi, O. S. (2020). Monosodium glutamate (MSG)-induced male reproductive dysfunction: A mini review. *Toxics*, *8*(1), 7.

Li, J., Tian, Y., Guo, S., Gu, H., Yuan, Q., & Xie, X. (2018). Testosterone-induced benign prostatic hyperplasia rat and dog as facile models to assess drugs targeting lower urinary tract symptoms. *PloS One*, *13*(1), e0191469.

Lim, K. B. (2017). Epidemiology of clinical benign prostatic hyperplasia. *Asian Journal of Urology*, *4*(3), 148–151. https://doi.org/10.1016/j.ajur.2017.06.004

McVary, K. T., Roehrborn, C. G., Avins, A. L., Barry, M. J., Bruskewitz, R. C., Donnell, R. F., Foster, H. E., Gonzalez, C. M., Kaplan, S. A., Penson, D. F., Ulchaker, J. C., & Wei, J. T. (2011). Update on AUA guideline on the management of benign prostatic hyperplasia. *The Journal of Urology*, *185*(5), 1793–1803. https://doi.org/10.1016/j.juro.2011.01.074

Meng, X.-Y., Zhang, H.-X., Mezei, M., & Cui, M. (2011). Molecular docking: A powerful approach for structure-based drug discovery. *Current Computer-Aided Drug Design*, *7*(2), 146–157.

Mjabri, B., Boucrot, P., & Aubry, J. (1992). The 1-O-octadecyl-2-O-methyl-sn-glycero-3-phosphocholine causes a differential incorporation of hexadecanol into neutral ether ester glycerolipids of 2 variant cell lines of rat colon carcinoma. *Archives Internationales De Physiologie, De Biochimie Et De Biophysique*, *100*(3), 237–240. https://doi.org/10.3109/13813459208998107

Mononen, N., Ikonen, T., Autio, V., Rökman, A., Matikainen, M. P., Tammela, T. L. J., Kallioniemi, O.-P., Koivisto, P. A., & Schleutker, J. (2002). Androgen receptor CAG polymorphism and prostate cancer risk. *Human Genetics*, *111*(2), 166–171. https://doi.org/10.1007/s00439-002-0776-5

Morgentaler, A., & Traish, A. M. (2009). Shifting the paradigm of testosterone and prostate cancer: The saturation model and the limits of androgen-dependent growth. *European Urology*, *55*(2), 310–320. https://doi.org/10.1016/j.eururo.2008.09.024

Morris, G. M., Huey, R., Lindstrom, W., Sanner, M. F., Belew, R. K., Goodsell, D. S., & Olson, A. J. (2009). AutoDock4 and AutoDockTools4: Automated docking with selective receptor flexibility. *Journal of Computational Chemistry*, *30*(16), 2785–2791. https://doi.org/10.1002/jcc.21256

Nicholson, T. M., Ricke, E. A., Marker, P. C., Miano, J. M., Mayer, R. D., Timms, B. G., Vom Saal, F. S., Wood, R. W., & Ricke, W. A. (2012). Testosterone and 17β-estradiol induce glandular prostatic growth, bladder outlet obstruction, and voiding dysfunction in male mice. *Endocrinology*, *153*(11), 5556–5565.

Nickel, J. C., Roehrborn, C., Montorsi, F., Wilson, T. H., & Rittmaster, R. S. (2011). Dutasteride reduces prostatitis symptoms compared with placebo in men enrolled in the REDUCE study. *The Journal of Urology*, *186*(4), 1313–1318. https://doi.org/10.1016/j.juro.2011.05.071

Obiri, D. D., Osafo, N., Oppong-Sarfo, J., & Prah, J. K. (2014). Margaritaria discoidea (Euphorbiaceae) stem bark extract attenuates allergy and Freund's adjuvant-induced arthritis in rodents. *Pharmacognosy Research*, *6*(2), 163–171. https://doi.org/10.4103/0974-8490.129039

Ogbu, P. N., Ugota, E. O., Onwuka, R. U., Ogbu, I. M., & Aloke, C. (2020). Effect of acetogenin fraction of Annona muricata leaves on antioxidant status and some indices

of benign prostatic hyperplasia in rats. *Redox Report*. https://www.tandfonline.com/doi/abs/10.1080/13510002.2020.1804711

Ogheneochuko, E. H., Chinazo, M.-I. C., & Emmanuel, P. D. (2024). Spermatogenic and Androgenic Potential of Nephrolepis biserrata on Testosterone- Propionate Induced Benign Prostatic Hyperplasia in Male Wistar Rats. *Journal of Applied Health Sciences and Medicine*. https://doi.org/10.58614/jahsm4104

Okeleji, L. O., Hamed, M. A., Jegede, A. I., Oyovwi, M. O., & Ajayi, A. F. (2025). Protective effects of coenzyme Q10 against trihexyphenidyl-induced testicular oxidative damage: modulation of antioxidant enzymes, inflammatory markers, hormonal and steroidogenic pathways in rats. *Steroids*, 109664.

Phua, T. J. (2021). The Etiology and Pathophysiology Genesis of Benign Prostatic Hyperplasia and Prostate Cancer: A New Perspective. *Medicines*, *8*(6), 30. https://doi.org/10.3390/medicines8060030

Pires, D. E., Blundell, T. L., & Ascher, D. B. (2015). pkCSM: Predicting small-molecule pharmacokinetic and toxicity properties using graph-based signatures. *Journal of Medicinal Chemistry*, *58*(9), 4066–4072.

Rastrelli, G., Corona, G., Vignozzi, L., Maseroli, E., Silverii, A., Monami, M., Mannucci, E., Forti, G., & Maggi, M. (2013). Serum PSA as a predictor of testosterone deficiency. *The Journal of Sexual Medicine*, *10*(10), 2518–2528.

Roehrborn, C. G. (2008). Pathology of benign prostatic hyperplasia. *International Journal of Impotence Research*, *20 Suppl 3*, S11-18. https://doi.org/10.1038/ijir.2008.55

Roehrborn, C. G., Siami, P., Barkin, J., Damião, R., Major-Walker, K., Nandy, I., Morrill, B. B., Gagnier, R. P., Montorsi, F., & CombAT Study Group. (2010). The effects of combination therapy with dutasteride and tamsulosin on clinical outcomes in men with

symptomatic benign prostatic hyperplasia: 4-year results from the CombAT study. *European Urology*, *57*(1), 123–131. https://doi.org/10.1016/j.eururo.2009.09.035

Shapiro, E., & Lepor, H. (1995). Pathophysiology of clinical benign prostatic hyperplasia. *The Urologic Clinics of North America*, *22*(2), 285–290.

Sofidiya, M. O., Orisaremi, C. O., Sansaliyu, I., & Adetunde, T. O. (2015). Gastroprotective and antioxidant potentials of ethanolic stem bark extract of Margaritaria discoidea (Euphorbiaceae) in rats. *Journal of Ethnopharmacology*, *171*, 240–246.

Tika, E., Ousset, M., Dannau, A., & Blanpain, C. (2019). Spatiotemporal regulation of multipotency during prostate development. *Development (Cambridge, England)*, *146*(20), dev180224. https://doi.org/10.1242/dev.180224

Trott, O., & Olson, A. J. (2010). AutoDock Vina: Improving the speed and accuracy of docking with a new scoring function, efficient optimization, and multithreading. *Journal of Computational Chemistry*, *31*(2), 455–461.

Van Der Sluis, T. M., Vis, A. N., Van Moorselaar, R. J. A., Bui, H. N., Blankenstein, M. A., Meuleman, E. J. H., & Heijboer, A. C. (2012). Intraprostatic testosterone and dihydrotestosterone. Part I: Concentrations and methods of determination in men with benign prostatic hyperplasia and prostate cancer. *BJU International*, *109*(2), 176–182. https://doi.org/10.1111/j.1464-410X.2011.10651.x

Veeresh Babu, S. V., Veeresh, B., Patil, A. A., & Warke, Y. B. (2010). Lauric acid and myristic acid prevent testosterone induced prostatic hyperplasia in rats. *European Journal of Pharmacology*, *626*(2), 262–265. https://doi.org/10.1016/j.ejphar.2009.09.037

Wang, F., Ma, D., Yang, J., Lyu, D., Gao, Q., Li, C., & Zhong, C. (2024). Mechanisms and Efficacy of Chinese Herbal Medicines in Benign Prostatic Hyperplasia. *Chinese Journal of Integrative Medicine*, *31*(1), Article 1. https://doi.org/10.1007/s11655-024-3916-0

Wellington, D., Mikaelian, I., & Singer, L. (2013). Comparison of ketamine–xylazine and ketamine–dexmedetomidine anesthesia and intraperitoneal tolerance in rats. *Journal of the American Association for Laboratory Animal Science*, *52*(4), 481–487.

Wilt, T., Ishani, A., Mac Donald, R., Rutks, I., & Stark, G. (2002). Pygeum africanum for benign prostatic hyperplasia. *The Cochrane Database of Systematic Reviews*, *1998*(1), CD001044. https://doi.org/10.1002/14651858.CD001044

Yang, H., Lou, C., Sun, L., Li, J., Cai, Y., Wang, Z., Li, W., Liu, G., & Tang, Y. (2019). admetSAR 2.0: Web-service for prediction and optimization of chemical ADMET properties. *Bioinformatics*, *35*(6), 1067–1069.

Young, S. (2021). Prostate artery embolization for benign prostatic hyperplasia: The hunt for the ideal patient population. *Diagnostic and Interventional Imaging*, *102*(3), 119–120. https://doi.org/10.1016/j.diii.2021.01.005

Zhou, Y., Xiao, X. Q., Chen, L. F., Yang, R., Shi, J. D., Du, X. L., Klocker, H., Park, I., Lee, C., & Zhang, J. (2009). Proliferation and phenotypic changes of stromal cells in response to varying estrogen/androgen levels in castrated rats. *Asian Journal of Andrology*, *11*(4), 451–459. https://doi.org/10.1038/aja.2009.28